

Theory of friction and boundary lubrication

B. N. J. Persson

Institut für Festkörperforschung, Forschungszentrum Jülich, Postfach 1913, D-52425 Jülich 1, Germany

(Received 9 February 1993; revised manuscript received 12 July 1993)

When an external force acts on an adsorbate structure, the structure may slide or flow relative to the substrate. The mechanism behind this sliding motion is of fundamental importance for the understanding of friction and lubrication between two flat macroscopic surfaces, and is also related to the question of what boundary condition should be used for the velocity field at a solid-liquid interface when solving the Navier-Stokes equations of fluid dynamics. Here I study the friction which occurs when adsorbate structures slide on surfaces. I present results of simulations based on Langevin or Brownian-motion dynamics, where the dependence of the linear sliding friction on the temperature and on the coverage is studied. I also present results for the nonlinear (in the external driving force) sliding friction, which is found to exhibit hysteresis giving rise to the well-known phenomenon of "stick-and-slip" motion. The theory predicts that for a class of sliding systems the ratio f_k/f_s between the kinetic and the static friction coefficient should equal $\frac{1}{2}$, in good agreement with experimental data.

I. INTRODUCTION

Tribology, the study of surfaces in moving contact, is a very important field technologically. But in spite of its technological importance, practically no understanding of friction from an atomistic level exists. Some fundamental questions are the following.

(1) What is the geometrical and electronic *structure* of the sliding interface?

(2) Where does the sliding *occur*?

(3) What is the *origin* of the sliding force?

Some more specific questions are the following.

(4) Why is usually the friction force F *proportional* to the load N ?

(5) Why in boundary lubrication (defined below) is the friction force F roughly *independent* of the sliding velocity v ?

(6) Why is the ratio f_k/f_s between the kinetic and the static friction coefficient close to $\frac{1}{2}$ for a large class of lubricated surfaces?

(7) What is the microscopic origin of "stick-and-slip" motion?

It is convenient to distinguish between hydrodynamic lubrication and boundary lubrication.¹ Hydrodynamic lubrication is used most frequently in bearings. The general idea is that if the lubricant is dragged through a convergent gap between the surfaces it will, on account of its finite viscosity, develop a pressure which may be high enough to keep the surfaces apart. The friction force can be calculated using the Navier-Stokes equations of hydrodynamics, and increases monotonically with increasing sliding velocity v .

If the velocity v becomes small enough the pressure generated in the lubricant is not high enough to support the journal and the two sliding surfaces may come in solid contact. In this case, in the contact region, the surfaces are separated by at most a few layers of lubrication molecules. This is the regime of boundary lubrication,

where the frictional forces usually are much higher (typically by a factor of 100) than in the hydrodynamic regime, and roughly independent of the sliding velocity v . In fact, if the load on the bearing is high enough the lubricant molecules may be completely removed from the contact area leading to a very high sliding friction and to wear. In order to avoid this, one usually gives some "additives" to the lubrication oil, e.g., fatty acids, which are long-chain hydrocarbons with a polar end group. These molecules will react with the solid surfaces and form a tightly held monolayer which is not removed even if the load on the bearing is very high. It is this monolayer which provides the main protection (reduced wear) and lubrication of the sliding surfaces. Note that the lubrication oil used in the hydrodynamic regime usually consist of hydrocarbons which do not interact as strongly with the solid surfaces as fatty acids.

In sliding friction measurements involving macroscopic bodies it is usually found that the friction force F is proportional to the normal load N , i.e.,

$$F \approx fN,$$

where f is the friction coefficient. There has been much speculations in the literature about the origin of this "law." One idea is based on the fact that most macroscopic bodies have a rough surface and that because of elastic and plastic deformations the actual contact area δA between the two bodies is proportional to the external load.² Hence one can speak about a frictional stress (friction force per unit area) $\sigma = F/\delta A$, and if $\delta A \sim N$ the friction law above follows immediately. Hence, σ rather than f is the fundamental quantity which has to be understood theoretically. In the measurements by Gee, McGuigan, and Israelachvili³ for "simple" lubricants between smooth mica surfaces, it has been proved that σ is independent of the external load, i.e., elastic deformation is the origin of the dependence of the friction force F

on the load N . On the other hand, for metals, plastic deformation is the main reason why $F \sim N$ (Ref. 4).

During sliding of clean (unlubricated) metal surfaces, the oxide film may be locally worn away and direct metal-to-metal contact can occur. The surface asperities weld together momentarily and are broken apart again to produce wear debris largely composed of metallic particles. This is called adhesive wear and is probably the main source of the friction force necessary to slide *clean* metal surfaces. It is obvious that this process gives a roughly velocity-independent sliding force since it depends only on the number of "collisions" between asperities occurring during sliding. However, in boundary lubrication the friction force is usually *not* determined by this mechanism since it is known experimentally from radioactive tracer experiments⁵ that while a boundary lubricant may reduce the sliding friction by a factor of ~ 10 , it may reduce the metallic transfer by a factor of 10^4 or more. Under these conditions the metallic junctions contribute very little to the friction force; the friction is due almost entirely to the force required to shear the lubricant film itself.

The study of the friction on an atomistic level has only very recently been started by solid-state physicists and chemists. New experimental techniques, such as the atomic force microscope or the quartz-crystal microbalance (QCM) studies of Krim *et al.*,³² and theoretical attempts to understand these results on an atomistic level by, e.g., molecular-dynamic simulations, has lead to a new research field called "atomic-scale friction" or "nanotribology." These and other studies have shown that friction can depend dramatically on the chemical and atomic nature of surfaces and can be extremely sensitive even to submonolayers of adsorbed atoms or molecules.⁶⁻¹³

In this paper I consider some simple sliding systems where, I believe, some of the questions raised above can be answered. In Sec. II, I define the model and present the basic equations from which the sliding friction $\bar{\eta}$ can be deduced. In Sec. III, I present a general discussion about the coverage and temperature dependence of the friction η which enters as an input parameter in the theory. In Sec. IV, I discuss the temperature and coverage dependence of the linear sliding friction. Section V presents a detailed study of the nonlinear (in the external driving force) sliding friction and in light of the theoretical results I discuss the friction measurements of Gee, McGuigan, and Israelachvili.³ Section VI presents a summary.

II. LANGEVIN OR BROWNIAN-MOTION DYNAMIC SIMULATIONS OF SLIDING OF ADSORBATE STRUCTURES

Consider now an adsorbate system and assume that in addition to the periodically corrugated adsorbate-substrate potential $U = \sum_i u(\mathbf{r}_i)$ and the adsorbate-adsorbate interaction potential $V = \frac{1}{2} \sum_{ij} v(\mathbf{r}_i - \mathbf{r}_j)$, an external force \mathbf{F} acts on each of the adsorbates. This will lead to a drift motion so that $m\bar{\eta}\langle \dot{\mathbf{r}} \rangle = \mathbf{F}$ where $\langle \rangle$ stands for thermal average and where \mathbf{r} denotes the coor-

dinate of an arbitrary adsorbate. For a weak external force \mathbf{F} , the sliding friction coefficient $\bar{\eta}$ is independent of \mathbf{F} .

We consider adsorbates on a (100) surface of a fcc crystal. The QCM measurement by Krim *et al.* was performed on evaporated silver films which have a (111) surface, but below we do not attempt a detailed quantitative comparison with the data of Krim *et al.* but rather emphasize general properties which should be independent of the substrate lattice structure and of the detailed form of U and V . The equation of motion for the particle coordinate $\mathbf{r}_i(t)$ taken to be

$$m\ddot{\mathbf{r}}_i + m\eta\dot{\mathbf{r}}_i = -\frac{\partial U}{\partial \mathbf{r}_i} - \frac{\partial V}{\partial \mathbf{r}_i} + \mathbf{f}_i + \mathbf{F}, \quad (1)$$

where \mathbf{F} is the external force introduced above and \mathbf{f}_i a stochastically fluctuating force which describes the influence on particle i from the irregular thermal motion of the substrate. The components f_i^α of \mathbf{f}_i are related to the friction η via the fluctuation-dissipation theorem

$$\langle f_i^\alpha(t) f_j^\beta(0) \rangle = 2\eta m k_B T \delta_{ij} \delta_{\alpha\beta} \delta(t). \quad (2)$$

For simplicity, I take

$$u(\mathbf{r}) = U_0 [2 - \cos(kx) - \cos(ky)] \quad (3)$$

so that $2U_0$ is the activation barrier for diffusion and $k = 2\pi/a$ where a is the "lattice" constant of the substrate. The adsorbate-adsorbate interaction potential V is taken as a sum of Lennard-Jones pair potentials

$$v(r) = \epsilon \left[\left(\frac{r_0}{r} \right)^{12} - 2 \left(\frac{r_0}{r} \right)^6 \right], \quad (4)$$

where ϵ is the well depth and r_0 the particle separation at the minima in the pair potential.

Equation (1) describes the motion of an adsorbate system on a corrugated substrate. When the external force $\mathbf{F} = \mathbf{0}$ the particle performs irregular motion (diffusion) with no long-time drift, i.e., $\langle \dot{\mathbf{r}} \rangle = \mathbf{0}$. For $\mathbf{F} > \mathbf{0}$, in addition to the irregular motion, the particles drift to the right with the speed $\langle \dot{\mathbf{r}} \rangle = \mathbf{F}/m\bar{\eta}$.

Let us first consider a limiting case. Assume that $U_0 \ll k_B T$. In this case we can neglect the periodic substrate potential in (1). Taking the thermal average of (1) and using $\langle \mathbf{f} \rangle = \mathbf{0}$ then gives

$$m \langle \ddot{\mathbf{r}} \rangle + m\eta \langle \dot{\mathbf{r}} \rangle = \mathbf{F}$$

or, since \mathbf{F} is constant,

$$m\eta \langle \dot{\mathbf{r}} \rangle = \mathbf{F}$$

so that $\bar{\eta} = \eta$ as expected in this case.

In order to study (1) in a general case, it is convenient to introduce dimensionless coordinates

$$\tilde{\mathbf{r}}_i = k\mathbf{r}_i, \quad \tilde{t} = t/\tau,$$

where

$$\tau = \left(\frac{m}{k_B T k^2} \right)^{1/2}.$$

In the new coordinates (1) becomes

$$\frac{d^2\tilde{\mathbf{r}}_i}{d\tilde{t}^2} + \tilde{\eta} \frac{d\tilde{\mathbf{r}}_i}{d\tilde{t}} = -\frac{\partial\tilde{U}}{\partial\tilde{\mathbf{r}}_i} - \frac{\partial\tilde{V}}{\partial\tilde{\mathbf{r}}_i} + \tilde{\mathbf{f}}_i + \tilde{\mathbf{F}}, \quad (5)$$

$$\langle \tilde{f}_i^\alpha(\tilde{t}) \tilde{f}_j^\beta(0) \rangle = 2\tilde{\eta} \delta_{\alpha\beta} \delta_{ij} \delta(\tilde{t}). \quad (6)$$

In these equations,

$$\tilde{u}(\tilde{\mathbf{r}}) = \tilde{U}_0(2 - \cos\tilde{x} - \cos\tilde{y})$$

and

$$\tilde{v}(\tilde{\mathbf{r}}) = \tilde{\epsilon} \left[\left(\frac{\tilde{r}_0}{\tilde{r}} \right)^{12} - 2 \left(\frac{\tilde{r}_0}{\tilde{r}} \right)^6 \right],$$

where

$$\tilde{\eta} = \eta\tau, \quad \tilde{r}_0 = kr_0, \quad \tilde{U}_0 = U_0/k_B T,$$

$$\tilde{\epsilon} = \epsilon/k_B T, \quad \tilde{\mathbf{F}} = \mathbf{F}/k_B T k.$$

In Secs. IV and V, I will present results for the sliding friction $\bar{\eta}$ obtained from computer simulations based on the Langevin equations (5) and (6). The random forces \mathbf{f}_i are assumed to form Gaussian random variables, generated by adding many random numbers which are equally distributed in the interval $[0,1]$. The time variable was discretized with the step length $\Delta=0.01\tau$ and the integration routine described by Schneider and Stoll¹⁴ was used in all the simulations. The basic unit was chosen as a square containing $M \times M$ substrate atoms where typically $M=10$. In the snapshot pictures of adsorbate structures shown below, it is assumed that the hollow sites have the largest adsorbate-substrate binding energy, i.e., these sites correspond to the local minima of $u(\mathbf{r})$ given by (3). If N denotes the number of adsorbates in the basic unit, then the coverage $\theta = N/(M \times M)$. In all simulations periodic boundary condition have been used. The system was “thermalized” by $\sim 10^6$ time steps which correspond to the actual “preparation” time $10^4\tau$; this was enough in all cases in order to reach thermal equilibrium. Figure 1 shows an example for $2U_0/\epsilon=2$ and $k_B T/\epsilon=1$, where $N=50$ particles initially are located in the lower part of the basic unit. Already after ~ 5000 time steps a $c(2 \times 2)$ structure is formed which is the thermal equilibrium structure for the coverage $\theta=0.5$ (the deviation of the adsorbates from the hollow sites is due to the thermally excited parallel adsorbate vibrations).

Equation (5) depends on the dimensionless parameters $2U_0/\epsilon$, $k_B T/\epsilon$, and a/r_0 . I have chosen the ratio a/r_0 to correspond to Xe on Ag(100); in this case $a=b/\sqrt{2}=2.89 \text{ \AA}$ (where b is the lattice constant of Ag) and $r_0=4.54 \text{ \AA}$ (the separation at the minimum in the Lennard-Jones pair potential) so that $r_0/a \approx 1.56$.

The drift friction $\bar{\eta}$ was obtained from the simulations using the definition $\bar{\eta} = F/m \langle v \rangle$ where F is an external force acting in the x direction on each adsorbate and which results in the adsorbate drift velocity $\langle v \rangle$, which was obtained from the simulations by averaging over all the particles in the basic unit and over many integration steps corresponding to the time $\sim 10^4\tau$.

$$2U_0/\epsilon = 2 \quad k_B T/\epsilon = 1$$

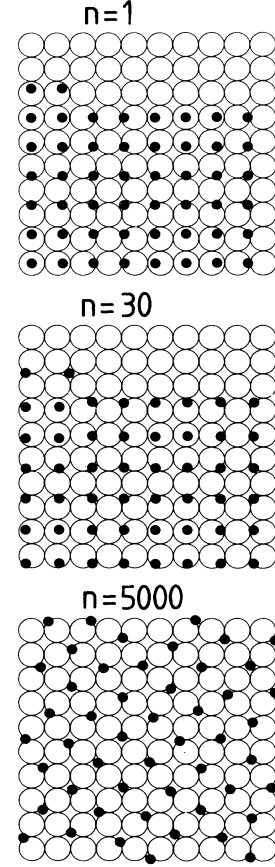


FIG. 1. Snapshot pictures (after $n=1, 30,$ and 5000 time steps) from Langevin dynamic simulations.

III. SOME COMMENTS ON THE FRICTION η

It is well known that the Langevin equation (1) cannot be microscopically correct. The frictional force on an adsorbate is ultimately due to “collisions” with the substrate ions and electrons, and takes the simple form $-m\eta\dot{\mathbf{r}}$ only on a time scale which is long compared to the frequency and duration of individual collisions.¹⁵ In general, one must replace

$$\eta\dot{\mathbf{r}}(t) \rightarrow \int_{-\infty}^t dt' \eta(t-t')\dot{\mathbf{r}}(t'). \quad (7)$$

In order to satisfy the fluctuation-dissipation theorem, the fluctuating force \mathbf{f} must satisfy

$$\langle f_\alpha(t) f_\beta(t') \rangle = mk_B T \delta_{\alpha\beta} \eta(t-t'). \quad (8)$$

The actual time dependence of the kernel $\eta(t)$ is determined by the nature of the adsorbate-substrate coupling; if the time scale introduced by this coupling is short compared with the time scale associated with the motion of the adsorbate, one may replace $\eta(t-t') \rightarrow 2\eta\delta(t-t')$ in which case one recovers the equations presented in Sec. II.

In principle, the friction kernel $\eta(t-t')$ depends also on $\mathbf{r}(t)$, and varies periodically parallel to the surface.

However, with respect to the electronic contribution to the friction, this dependence is probably negligible for the systems studied by Krim *et al.*; the "corrugation" of η_{eh} is likely to be of similar magnitude as the corrugation in the binding energy which is of order 10% or less for these systems. The corrugation of the phonon contribution may be larger, as discussed below.

Let us first consider the electronic friction. I will show that using a "local" friction $\eta_{eh}(t-t') \rightarrow 2\eta_{eh}\delta(t-t')$ is an excellent approximation and furthermore that η_{eh} is practically temperature independent. Let us consider a forced oscillation

$$\mathbf{r}(t) = \mathbf{r}_0 + \mathbf{a}(e^{-i\omega t} + e^{i\omega t}). \quad (9)$$

The energy dissipation per unit time caused by the frictional force can be written as

$$\begin{aligned} P &= m \int_{-\infty}^t dt' \eta(t-t') \dot{\mathbf{r}}(t') \cdot \dot{\mathbf{r}}(t) \\ &= m \mathbf{a}^2 \omega^2 \eta(\omega), \end{aligned} \quad (10)$$

where

$$\eta(\omega) = \int_0^{\infty} dt \eta(t) e^{-i\omega t}.$$

In (10) I have performed a time average which eliminates the terms proportional to $\exp(\pm 2i\omega t)$. If \mathbf{a} is small, we can evaluate the power absorption directly using the golden-rule formula. The most general form of the coupling between an adsorbate and the electronic excitations of the substrate is

$$H' = \sum_{\alpha\beta} \mathbf{r} \cdot \mathbf{A}_{\alpha\beta} c_{\beta}^{\dagger} c_{\alpha},$$

where c_{α}^{\dagger} and c_{α} are the creation and annihilation operators for electrons in the one-particle state $|\alpha\rangle$, which is assumed to be an eigenstate of H_0 . Using the golden-rule formula, and accounting for both stimulated absorption and emission, gives

$$\begin{aligned} P &= 2\pi\omega \sum_{\alpha\beta} [n_{\alpha}(1-n_{\beta}) - n_{\beta}(1-n_{\alpha})] |\mathbf{a} \cdot \mathbf{A}_{\alpha\beta}|^2 \\ &\quad \times \delta(\epsilon_{\alpha} + \omega - \epsilon_{\beta}) \\ &= 2\pi\omega \sum_{\alpha\beta} (n_{\alpha} - n_{\beta}) |\mathbf{a} \cdot \mathbf{A}_{\alpha\beta}|^2 \delta(\epsilon_{\alpha} + \omega - \epsilon_{\beta}), \end{aligned}$$

where n_{α} is the occupation of orbital $|\alpha\rangle$. Let us introduce

$$F(\epsilon, \omega) = \sum_{\alpha\beta} \delta(\epsilon - \epsilon_{\alpha}) \delta(\epsilon + \omega - \epsilon_{\beta}) |\mathbf{a} \cdot \mathbf{A}_{\alpha\beta}|^2$$

so that

$$P = 2\pi\omega \int d\epsilon [n(\epsilon) - n(\epsilon + \omega)] F(\epsilon, \omega),$$

where

$$n(\epsilon) = (e^{\beta(\epsilon - \epsilon_F)} + 1)^{-1}$$

is the Fermi-Dirac distribution function. Now, the function $F(\epsilon, \omega)$ is expected to vary slowly with ϵ in the narrow energy interval where the factor $[n(\epsilon) - n(\epsilon + \omega)]$ is nonvanishing. The width of this interval is of the order

of $\max(k_B T, \omega)$, and since we only are interested of very small frequencies ω , of order $k_B T$ or smaller, we can expand $F(\epsilon, \omega) \approx F(\epsilon_F, 0) + a(\epsilon - \epsilon_F)/\epsilon_F + b\omega/\epsilon_F + \dots$, where a and b are constants of order unity. Since

$$\int d\epsilon [n(\epsilon) - n(\epsilon + \omega)] = \omega$$

we get

$$P = 2\pi\omega^2 [F(\epsilon_F, 0) + ak_B T/\epsilon_F + b\omega/\epsilon_F + \dots]. \quad (11)$$

Comparing (10) with (11) we conclude that, to an excellent approximation, $\eta_{eh}(\omega)$ is both frequency and temperature independent, with the leading corrections being of order ω/ϵ_F and $k_B T/\epsilon_F$ and completely negligible. Note that this result is consistent with the Xe/Ag(111) data of Krim *et al.*, where the sliding friction was found to be temperature independent at incommensurate coverages.¹⁶

Let us now turn to the phonon friction η_{ph} . For an isolated adsorbate, we can determine $\eta_{ph}(\omega)$ by evaluating the energy dissipation rate associated with a small-amplitude adsorbate vibration as in (9), and equating this with (10). Since the force on the substrate ions, as the adsorbate vibrates according to Eq. (9), may vary appreciably with the position of the adsorbate in the substrate unit cell, it follows that η_{ph} may exhibit a non-negligible dependence of \mathbf{r} , even for the weak-absorption systems considered by Krim *et al.*¹⁷ At substrate symmetry sites we may estimate η_{eh} using¹⁸

$$\eta_{ph} = 0.12 \frac{m}{\rho} \left[\frac{\omega_0}{c_T} \right]^3 \omega_0, \quad (12)$$

where ρ and c_T are the substrate mass density and the transverse sound velocity, respectively. The frequency ω_0 is the frequency of small-amplitude vibrations at the symmetry site in question. We estimate ω_0 using the form of $u(\mathbf{r})$ given in Sec. II. Expanding $u(\mathbf{r})$ to quadratic order in \mathbf{r} gives

$$u(\mathbf{r}) = U_0 [2 - \cos(kx) - \cos(ky)] \approx U_0 k^2 \mathbf{r}^2 / 2$$

and

$$\frac{1}{2} m \omega_0^2 \mathbf{r}^2 \approx \frac{1}{2} U_0 \left[\frac{2\pi}{a} \right]^2 \mathbf{r}^2$$

or

$$\omega_0 \approx \frac{2\pi}{a} \left[\frac{U_0}{m} \right]^{1/2}. \quad (13)$$

For Xe on Ag(111) with $2U_0 = 10$ meV this formula gives $\omega_0 \approx 6$ cm⁻¹ and from (12) the phononic friction $\eta_{ph} \approx 4 \times 10^7$ s⁻¹, which is roughly one order of magnitude smaller than the electronic friction deduced from surface resistivity measurements (see Ref. 19). This estimate of the phononic friction is quite rough, but is consistent with our earlier conclusion²⁰ that the electronic friction is very important for the sliding friction for the systems studied by Krim *et al.*

Equation (12) is based on a continuum treatment of the substrate and holds only if "typical" frequencies involved in the adsorbate motion are small compared with the Debye frequency of the substrate. For the adsorbate sys-

tems considered by Krim *et al.* these typical frequencies are of order $\omega_0 \sim 10 \text{ cm}^{-1}$ or of order $v_{\text{th}}/a \sim 10 \text{ cm}^{-1}$, both of which are much smaller than the Debye frequency ω_D of approximately a few hundred cm^{-1} . Hence this condition is rather well satisfied. Note that in this limit η_{ph} is both frequency and temperature independent. More generally, η_{ph} is temperature independent as long as only one-phonon processes are involved (multiphonon processes introduces a temperature dependence). But η_{ph} is frequency independent only as long as $\omega \ll \omega_D$, even if only one-phonon processes are involved.

Let us now briefly discuss the electronic and phononic contributions to the sliding friction of incommensurate adsorbate systems.

Surface resistivity data indicate that η_{eh} is typically 30–50 % smaller at incommensurate adsorbate coverages as compared with low adsorbate coverages. Note that in these measurements, the adsorbate structure as a whole “move” relative to the electronic system, i.e., exactly the same type of motion which occur during the sliding friction measurements of Krim *et al.* The relative small change in the electronic friction between low and high coverages is in accordance with what one would expect from theory.

The situation is drastically different with respect to the phononic friction. It has been shown by Aubry and Andry²¹ and by Sokoloff²² that the phononic friction during sliding of incommensurate structures is extremely small and in particular vanishes if the substrate pinning potential can be neglected. Nevertheless, Sokoloff has shown that a small concentration of point imperfections can give a phonon contribution which can account for the damping observed in the QCM experiments.²³

IV. LINEAR SLIDING FRICTION

In this section I study the linear (in the external driving force F) sliding friction $\bar{\eta}$. For the adsorbate systems studied by Krim *et al.* the friction η is very small and in this case it can be shown that $\bar{\eta}$ is directly proportional to η . In the simulations reported on below I have chosen $\bar{F}=0.05$ and $\bar{\eta}=0.1$ which essentially correspond to the linear response and low friction limits where $\bar{\eta}/\eta$ is independent of F and η ; this limit is directly relevant for the interpretation of the experimental data of Krim *et al.*

Figures 2(a) and 2(b) show the adsorbate phase diagrams for $2U_0/\epsilon=0.5$ and 2.0, respectively. In the former case, the substrate corrugation is so weak that the phase diagram is essentially that of a two-dimensional Lennard-Jones system on a *flat* surface²⁴ (note, no extensive study of the exact location of the phase boundaries has been undertaken and those indicated in Fig. 2 are obtained with a $M=10$ basic unit; however, this is not important for what follows). In the figure F , IC , G , and L denote the fluid phase, the incommensurate solid phase, the gas and liquid phases, respectively; the gas and liquid phases are the fluid phase at low and high density, respectively. Similarly, $G+L$ and $G+IC$ denote the gas-liquid and gas-incommensurate solid coexistence regions, respectively. The phase diagram in Fig. 2(b)

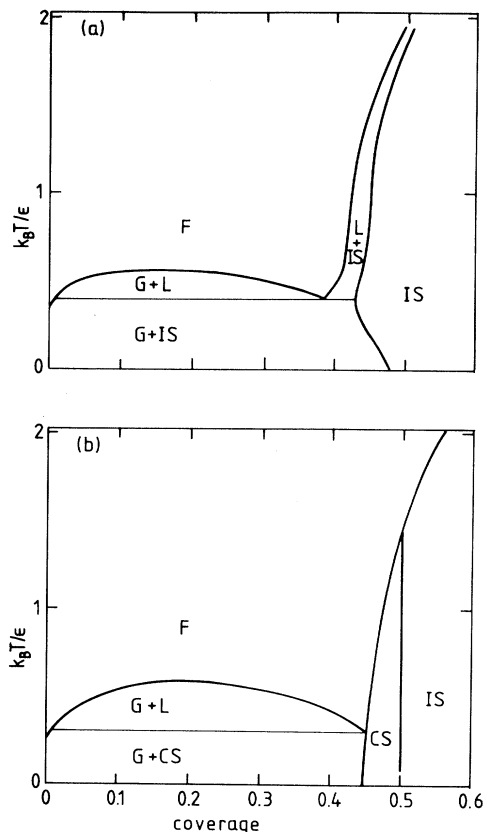


FIG. 2. The adsorbate phase diagram for (a) $2U_0/\epsilon=0.5$ and (b) $2U_0/\epsilon=2.0$. The phase boundaries are only roughly correct and obtained for a $M=10$ basic unit. In the figure F , G , L , IS , and CS denotes fluid, gas, liquid, incommensurate solid, and commensurate solid, respectively.

differs most importantly from that in 2(a) by a new phase around the coverage $\theta=0.5$. This phase, a $c(2 \times 2)$ commensurate solid (CS) phase, is shown in Fig. 5(b) below. It is obvious that this structure is stable if $2U_0/\epsilon$ is large enough because all adsorbates bind at hollow sites, i.e., the adsorbate-substrate binding energy is maximized while the separation between nearby adsorbates is close to the equilibrium separation in the pair potential $v(r)$. But in Fig. 2(a) the corrugation of the substrate potential is so weak that the adsorbates prefer to minimize the adsorbate-adsorbate interaction energy by forming a triangular incommensurate solid phase, see Fig. 5(a).

For later use, let me discuss the nature of the transition between the “low”-temperature $c(2 \times 2)$ structure and the “high”-temperature fluid structure at $\theta=0.5$. In Fig. 3, I show the result for $\eta/\bar{\eta}$ as the temperature is reduced from above T_c to below, where T_c is the *fluid* \leftrightarrow $c(2 \times 2)$ phase transition temperature. Note that $\eta/\bar{\eta}$ equals the ratio $\langle v \rangle/v_0$ between the actual drift velocity $\langle v \rangle$ (for the corrugated substrate under consideration) and the drift velocity v_0 which would occur if the surface were flat. This result follows directly from the definitions $m\bar{\eta}\langle v \rangle = F$ and $m\eta v_0 = F$, which give $\eta/\bar{\eta} = \langle v \rangle/v_0$. From the figure we conclude that $k_B T_c \approx 1.2\epsilon$ and that

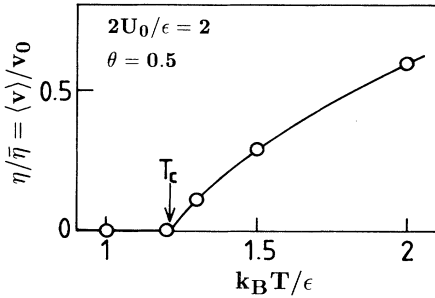


FIG. 3. The inverse of the normalized drift friction, $\eta/\bar{\eta}$ (equal to the normalized drift velocity $\langle v \rangle/v_0$), as a function of temperature for $\theta=0.5$ and $2U_0/\epsilon=2$. The melting temperature of the $c(2 \times 2)$ structure is at $k_B T_c = 1.2\epsilon$.

the transition is continuous; symmetry arguments show that the transition is in the Ising universality class. The result in Fig. 3 has been obtained with an external force $\bar{F}=0.05$, but this force is so weak that it has a negligible influence on T_c .

In Fig. 4, I show the result for $\eta/\bar{\eta}$ as a function of coverage and for a few different temperatures. Let us first consider the case of a “low”-corrugated adsorbate-substrate interaction potential, $2U_0/\epsilon=0.5$, see Fig. 4(a).

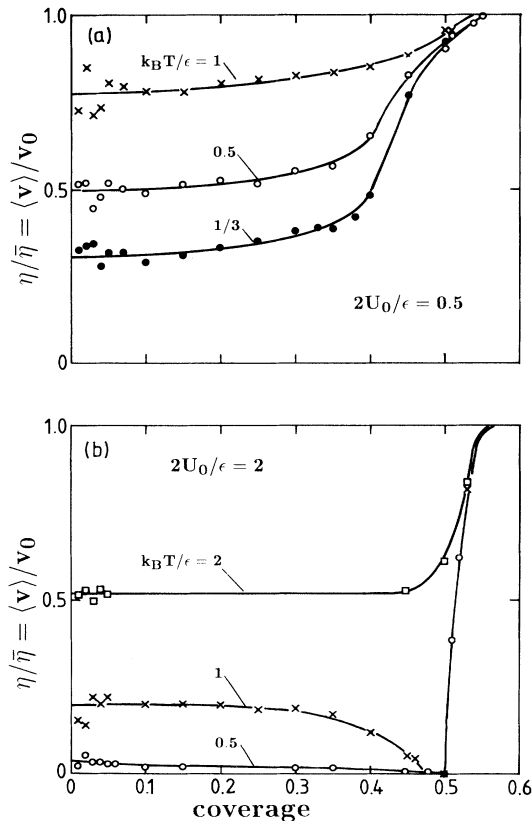


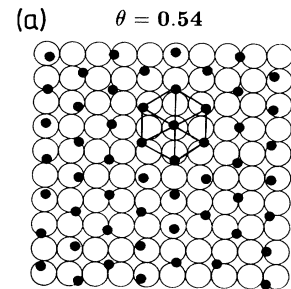
FIG. 4. The inverse of the normalized drift friction, $\eta/\bar{\eta}$ (equal to the normalized drift velocity $\langle v \rangle/v_0$), as a function of coverage for several different temperatures. (a) $2U_0/\epsilon=0.5$ and (b) $2U_0/\epsilon=2.0$.

In this case, as the coverage increases, the sliding velocity $\langle v \rangle$ increases monotonically towards v_0 . For large coverages the adsorbate system is dominated by the adsorbate-adsorbate interaction and a practically perfect triangular adsorbate structure is formed, as shown by the snapshot picture in Fig. 5(a) (for $\theta=0.54$ and $k_B T/\epsilon=0.5$). This structure can slide (collectively) practically without any activation barriers on the substrate, since as some adsorbates move uphill during sliding, other adsorbates moves downhill. Hence, the *pinning* potential induced by the substrate is negligible in this case and $\langle v \rangle \approx v_0$. This also explains why $\langle v \rangle$ is almost temperature independent for $\theta > 0.55$ —the barriers which must be overcome during sliding are very small and can be neglected.

On the other hand, for low adsorbate coverage, $\langle v \rangle$ is much smaller than v_0 and strongly temperature dependent. This is easy to understand in the limit of very low adsorbate coverage where a dilute lattice gas occurs—here each adsorbate atom performs an independent random walk type of motion with a slight drift in the direction of the weak external force F . The particles have to “jump” over the barriers $\sim 2U_0$ separating the different local minima on the potential energy surface and this is a thermally activated process, the rate of which, at low temperature, is proportional to $\sim \exp(-2U_0/k_B T)$. Note that the external force F is much too weak to by itself “move” adsorbates over the barriers in the system (except for incommensurate structures).

Between the low-coverage region and the region where

$2U_0/\epsilon = 0.5 \quad k_B T/\epsilon = 0.5$



$2U_0/\epsilon = 2 \quad \theta = 0.5$

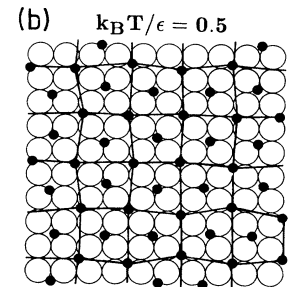


FIG. 5. Snapshot pictures of the adsorbate structure for (a) $2U_0/\epsilon=0.5$ and $\theta=0.54$ where a triangular incommensurate structure occur and (b) $2U_0/\epsilon=2.0$ and $\theta=0.5$ where a commensurate $c(2 \times 2)$ structure occur. In both cases $k_B T=0.5\epsilon$.

the sharp increase in $\langle v \rangle/v_0$ occurs, i.e., for $\theta < 0.4$, there is a weak monotonic increase of $\langle v \rangle$ with increasing θ , in particular at low temperature. This can be understood as a result of a monotonic increase in the fraction of adsorbates which occur in the incommensurate solid or in the dense liquid phase, as the coverage increases and by the fact that the latter structures slide easier than the isolated adsorbates which occur in the lattice gas surrounding these "islands" of condensate.

Let us now consider the case of a "strongly" corrugated substrate, $2U_0/\epsilon=2$, see Fig. 4(b). Again, at high coverage $\langle v \rangle \rightarrow v_0$. That is, at high enough coverages the adsorbate-adsorbate interaction dominates over the adsorbate-substrate interaction and the pinning potential is negligible. Note, however, that in the present case it is necessary to go to slightly higher coverages than for $2U_0/\epsilon=0.5$, before one enters into the incommensurate solid-phase region; this is exactly what one would expect when the corrugation of the adsorbate-substrate interaction potential increases. (In practice it may be impossible to reach those high coverages where $\langle v \rangle \approx v_0$ before desorption or multilayer absorption occur.)

The drift velocity for very low adsorbate coverages, where a dilute lattice gas exists, is of exactly the same nature in the present case as in the earlier case where $2U_0/\epsilon=0.5$ (see above). But if $k_B T < 1.2\epsilon$, the drift velocity *decreases* continuously with increasing coverage up to $\theta=0.5$. At $\theta=0.5$ the drift velocity is extremely low, in particular at low temperatures; the reason is obvious if one considers a snapshot picture of the adsorbate system at this coverage, see Fig. 5(b). Obviously, except for thermal displacements of the adsorbates away from the hollow sites, a perfect $c(2 \times 2)$ structure occurs. This structure is strongly pinned by the adsorbate-substrate interaction. In principle, elementary excitations can be thermally excited in the $c(2 \times 2)$ structure and drift in the direction of the applied force F , but in the present system these excitations have a very high energy and will occur only in a negligible concentration. The point is that moving an adsorbate from a hollow site to any of the nearby empty hollow sites leads to a very strong increase in the adsorbate-adsorbate repulsion energy. This will effectively block the movement of the adsorbates and lead to a very low drift velocity. But for coverages just slightly higher than 0.5, the adsorbate system undergoes a phase transition to the incommensurate triangular structure shown in Fig. 5(a) for which the pinning potential is small.

The continuous decrease in the sliding velocity as θ increases towards 0.5 is caused by fluctuations, i.e., for $\theta < 0.5$ but close to the region where the $c(2 \times 2)$ structure occurs, patches of the $c(2 \times 2)$ structure occur in a fluidlike phase. These patches are pinned stronger by the substrate potential than isolated adsorbates and this consequently reduces the drift velocity. For the weaker corrugated substrate, $2U_0/\epsilon=0.5$, the $c(2 \times 2)$ structure does not occur and, as discussed above, the sliding velocity increases continuously with increasing coverage. Note also that for $k_B T > 1.2\epsilon$ no $c(2 \times 2)$ structure occurs even in the present case and sliding friction increases monotonically with increasing coverage.

V. NONLINEAR SLIDING FRICTION — "STICK-AND-SLIP" MOTION

In this section I consider the nonlinear sliding friction which is relevant for "practical" sliding systems, e.g., when a block slides on a flat surface with an intervening layer of lubrication molecules (boundary lubrication). Such a system often exhibit "stick-and-slip" motion which can be understood based on the nonlinear nature of the sliding friction (see below); within linear response "stick-and-slip" is absent.

We consider the same adsorbate systems as in Sec. IV but now with an arbitrary strong force F acting on each adsorbate. In Fig. 6, I show $\langle v \rangle/v_0 = \eta/\bar{\eta}$ as a function of F for a "strongly" corrugated substrate, $2U_0/\epsilon=2$. In Fig. 6(a), the coverage $\theta=0.25$ and results are presented for two temperatures, $k_B T/\epsilon=0.5$ (circles) and 1.0 (squares). In both cases the overlayer is in a fluid state even for $F=0$. Note that for $\bar{F} > 0.6$, the adsorbate structure slides as if there were no barriers to overcome on the surface, i.e., $\langle v \rangle \approx v_0$. In fact, as shown in Appendix A, as $F \rightarrow \infty$,

$$\langle v \rangle \sim v_0 \left[1 - \frac{1}{4} U_0^2 m^2 \left(\frac{\eta}{F} \right)^4 \right]$$

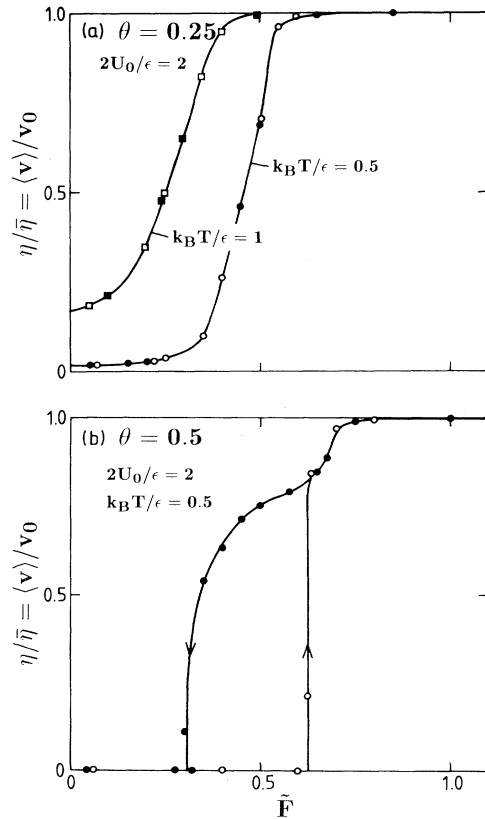


FIG. 6. The drift velocity $\langle v \rangle$ as a function of the external force F acting on each adsorbate for $2U_0/\epsilon=2.0$. (a) $\theta=0.25$ and (b) $\theta=0.5$. The open and filled circles are obtained by increasing the force F from zero and by reducing F from a high value, respectively.

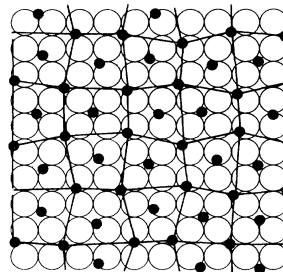
to leading order in $1/F$. Note also that for $\tilde{F} < 0.6$, when the temperature is increased, the sliding velocity $\langle v \rangle$ increases; this result is obvious since at the higher temperature the thermal motion of the substrate ions and electrons [as manifested by the fluctuating force f_i in (1)] is stronger and they will more frequently kick the adsorbates over the barriers in the system. The open and filled circles (and squares) are obtained by increasing the force F from zero and by reducing the force F from a high value, respectively. More precisely, the open circles (and squares) have been obtained as follows. (a) The system is first “thermalized” with $F=0$ for about $\sim 10^6$ time steps. (b) Next, the force F is instantaneously increased to its final value and another $\sim 10^6$ time steps were performed in order to reach a steady state. (c) Finally, $\langle v \rangle$ is obtained by averaging over all the particles in the basic unit cell and over $\sim 10^6$ additional time steps. The filled circles was obtained in a similar way, except that (a) was replaced by a “thermalization” of the system at a high force, $\tilde{F} \sim 1$. But in the present case both procedures gives identical results, i.e., no hysteresis occurs. More generally, whenever the adsorbate system (for $F=0$) is in a fluid state, no hysteresis is observed. But if a (commensurate) solid phase occurs, the sliding friction exhibits hysteresis. This is illustrated in Fig. 6(b) which shows the result of simulations for $\theta=0.5$ and $k_B T/\epsilon=0.5$, where the $c(2 \times 2)$ structure shown in Fig. 5(b) prevails when $F=0$ [see the phase diagram, Fig. 2(b)]. In this case a large hysteresis occurs: Initially, as the force F increases from zero, the ordered $c(2 \times 2)$ structure prevails and the sliding velocity vanishes, $\langle v \rangle = 0$, until \tilde{F} reaches $\tilde{F}_0 \approx 0.6$. At $F=F_0$, the sliding velocity $\langle v \rangle$ increases abruptly and inspection of the adsorbate structures shows that it has changed from the $c(2 \times 2)$ structure which occurs for $F < F_0$ to a fluidlike state for $F > F_0$, see Fig. 7. But when the system is first “thermalized” with a large force, $\tilde{F} \sim 1$, and then F reduced, the system does not flip back to the $c(2 \times 2)$ structure until $\tilde{F} = \tilde{F}_1 \approx 0.3$. Again, inspection of adsorbate structures shows that for $F > F_1$ the system is fluidlike while for $F < F_1$ the $c(2 \times 2)$ structure prevails. These results are completely general—*whenever a solid commensurate adsorbate structure occurs, the $\langle v \rangle = f(F)$ relation exhibits hysteresis*. This is probably also the case even if the substrate is disordered, e.g., in a glassy state, as long as a solid adsorbate structure occurs for $F=0$.

In Fig. 8, I show the relation between \tilde{F} and $\langle \tilde{v} \rangle$ as obtained from Fig. 6. The dashed line is the result obtained if the substrate were uncorrugated, i.e., it is determined by $\tilde{\eta} \langle \tilde{v} \rangle = \tilde{F}$.

The structure of the $\langle v \rangle = f(F)$ curve implies “stick-and-slip” motion of macroscopic bodies. To see this, consider a block on a substrate and assume that a spring is attached to one end of the block, and that the other end of the spring is pulled with the constant velocity v . If v is smaller than v_c , where $v_c > 0$ is the lowest possible (nonzero) sliding velocity of the lubricant layer [see Fig. 8(b)], then no stationary (i.e., constant velocity) sliding motion of the block is possible. This follows at once from the fact that there is a “velocity gap” $0 < v < v_c$ in the $v = f(F)$ curve, i.e., a velocity region where no stationary

$$2U_0/\epsilon = 2 \quad \theta = 0.5$$

$$(a) \quad \tilde{F} = 0.6$$



$$(b) \quad \tilde{F} = 0.65$$

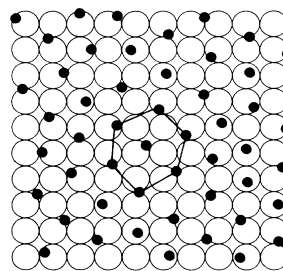


FIG. 7. Snapshot pictures of the adsorbate structure for $\theta=0.5$ as obtained by increasing the force F from zero. (a) $F=0.6$ and (b) $F=0.65$.

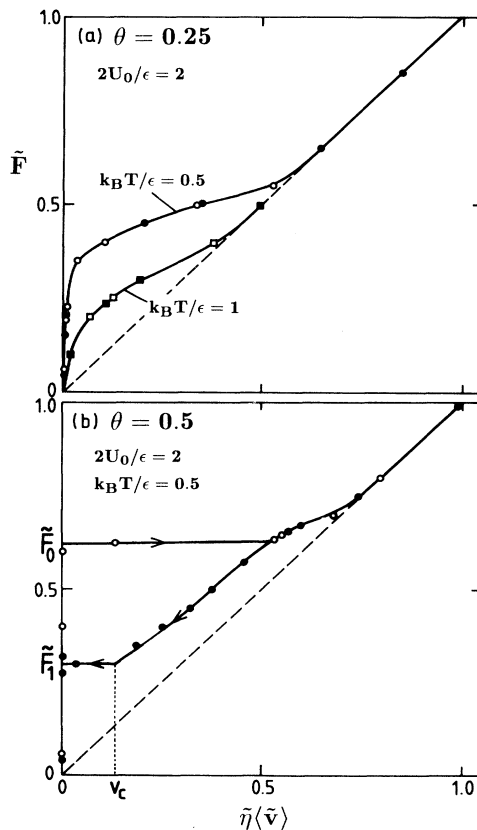


FIG. 8. The relation between $\langle v \rangle$ and the force F obtained from Fig. 6.

(i.e., constant velocity) motion of the lubrication film is possible. Hence, the actual motion will decompose itself into a stick period and a slip period in such a way that the average velocity of the block equals the spring velocity v . Note that the spring in this discussion could represent the elastic properties of the block itself, i.e., it does not need to be an “external” spring.

From the discussion above it follows that only when a solid phase occurs (when $F=0$) does one expect to find “stick-and-slip” motion, in good agreement with experiment.^{7,8} No “stick-and-slip” motion is observed when the lubricant is in a fluid state.

A deeper insight into the numerical results presented above for the nonlinear sliding friction can be obtained based on the following results. It is well known that a stationary solid object imbedded in a flowing fluid gives rise to energy dissipation. That is, collective translational energy of the fluid is converted into irregular motion finally leading to a heating of the fluid. Now, the same thing happens for a fluid adsorbate layer under the influence of an external force \mathbf{F} . The external force $\mathbf{F}=\tilde{F}\hat{\mathbf{x}}$ accelerates the adsorbates in the x direction but due to “scattering” from the corrugated substrate potential $u(\mathbf{r})$ and due to the adsorbate-adsorbate interaction (as manifested in the viscosity of the fluid), “drift momentum” is transferred into irregular motion. In the absence of thermal contact to a heat bath [i.e., with $\eta=0$ in (1)] this “scrambling” of momentum would lead to a continuous increase of the temperature of the two-dimensional fluid. But in the present case, owing to the thermal contact to the substrate (at temperature T), energy will flow to the substrate at a rate which, when steady state has been reached, must equal the power transferred to the adsorbate system from the external force F . Using this fact, one can derive an expression for the effective temperature T^* of the adsorbate system as follows: The power (per adsorbate) transferred to the adsorbate system from the external force is

$$P = \mathbf{F} \cdot \langle \mathbf{v} \rangle = F^2 / m \bar{\eta}, \quad (14)$$

where the last equality follows from the definition $m \bar{\eta} \langle \mathbf{v} \rangle = \mathbf{F}$. But, at steady state, this power must equal that transferred from the adsorbate system to the substrate which has two contributions, namely, a term $\alpha(T^* - T)$ proportional to the difference in temperature between the film and the substrate and another term, $m \eta \langle v^2 \rangle$, which describes the direct energy transfer to the substrate (via the friction η) from the drift motion of the adsorbate system. Hence,

$$P = \alpha(T^* - T) + m \eta \langle v^2 \rangle. \quad (15)$$

The heat transfer coefficient α can be derived as follows. Assume that $F=0$ and $T=0$ and that the adsorbate system has the temperature T^* . The energy flow from the adsorbate system to the substrate is then determined by the friction force, $-m \eta \mathbf{v}$, acting on each adsorbate, and the average energy dissipation is therefore $m \eta \langle v^2 \rangle$ which must equal αT^* . Since $k_B T^* = m \langle v^2 \rangle / 2$ this gives $\alpha = 2k_B \eta$. Substituting this in (15) and comparing with (14) gives

$$k_B T^* = k_B T + \frac{F^2}{2m \eta \bar{\eta}} \left[1 - \frac{\eta}{\bar{\eta}} \right]. \quad (16)$$

In the dimensionless variables introduced in Sec. II this equation takes the form

$$\frac{T^*}{T} = 1 + \frac{\tilde{F}^2}{2\bar{\eta}^2} \left[1 - \frac{\eta}{\bar{\eta}} \right] \frac{\eta}{\bar{\eta}}. \quad (17)$$

The circles in Fig. 9 show T^*/T as a function of \tilde{F} as obtained from (17) and Fig. 6 (the filled circle on the dashed line is obtained from the sliding friction of the metastable fluid in Figs. 16 and 18 below). But the temperature T^* can also be obtained directly from the simulations as follows. Let us write the velocity of an adsorbate as

$$\mathbf{v} = \langle \mathbf{v} \rangle + \delta \mathbf{v},$$

where $\langle \delta \mathbf{v} \rangle = \mathbf{0}$. Hence,

$$\langle v^2 \rangle = \langle \mathbf{v} \rangle^2 + \langle (\delta \mathbf{v})^2 \rangle.$$

Now, if the motion $\delta \mathbf{v}$ is to correspond to the adsorbate temperature T^* then $k_B T^* = m \langle (\delta \mathbf{v})^2 \rangle / 2$ so that

$$k_B T^* = m (\langle v^2 \rangle - \langle \mathbf{v} \rangle^2) / 2. \quad (18)$$

The temperature deduced using this equation agrees within the “noise” of the simulations with those deduced from Eq. (17). For example, for $\tilde{F}=0.42$ Eq. (17) gives $T^*/T=2.952$ while (18) gives $T^*/T=2.942$. In order for the motion $\delta \mathbf{v}(t)$ to really correspond to a temperature it is necessary to show that both δv_y and δv_x have Maxwellian probability distributions of equal width, i.e.,

$$P_x(v_x) = \left[\frac{m}{2\pi k_B T^*} \right]^{1/2} e^{-m(v_x - \langle v_x \rangle)^2 / 2k_B T^*},$$

$$P_y(v_y) = \left[\frac{m}{2\pi k_B T^*} \right]^{1/2} e^{-mv_y^2 / 2k_B T^*}.$$

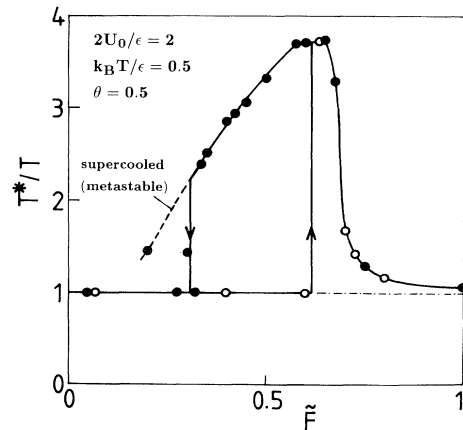


FIG. 9. The effective temperature T^* in the overlayer in units of the substrate temperature T , as a function of the force \tilde{F} . In the calculation $2U_0/\epsilon=2$ and $k_B T/\epsilon=0.5$. The data point on the dashed line is deduced from Fig. 16.

That this indeed is the case is shown in Fig. 10 for $\bar{F}=0.45$. Equally good Maxwellian distributions are found for all other values of F and the effective temperature T^* deduced from the width of the probability distributions P_x and P_y never deviates by more than 3%.

From Fig. 9 it is seen that the transition from the fluid state to the pinned $c(2 \times 2)$ structure occurs when the temperature T^* in the overlayer reaches $2.4T$ or $k_B T^* = 1.2\epsilon$, since $k_B T/\epsilon = 0.5$ in the present simulations. But $T^* = 1.2\epsilon/k_B$ is identical to the melting temperature T_c of the $c(2 \times 2)$ structure (see Fig. 3), i.e., the return to the pinned structure (at $F = F_1$) occurs when the temperature T^* in the overlayer reaches the melting temperature T_c . This is not an "accidental" result but I will argue below that it occurs whenever the temperature T^* in the overlayer exceeds T_c when $F = F_0/2$. For example, in Fig. 11(a), I show the effective temperature T^* in a simulation performed at a lower substrate temperature than above, namely, $k_B T/\epsilon = 0.4$ instead of 0.5 as above but still for $2U_0/\epsilon = 2$.

The return to the pinned structure (at $F = F_1$) can occur under two kinds of conditions: (a) when the adsorbate temperature $T^* \approx T_c$ as in the simulation presented above or (b) when $F \approx F_0/2$. Case (a) occurs if T^* is above T_c when $F \approx F_0/2$ while (b) occurs if this condition is not met. Note that η is proportional to the adsorbate-substrate heat transfer coefficient and if η increases the

temperature in the adsorbate layer decreases. Hence, for large enough η , $T^* < T_c$ and consequently $F_1 \approx F_0/2$. I will show below that this result holds independent of the detailed form of the adsorbate-adsorbate and adsorbate-substrate interactions; it represents the most important result obtained in this paper and explains why for a large class of sliding systems the ratio between the kinetic f_k and the static f_s friction coefficients is approximately equal to 0.5 (see below).

I will now address the fundamental questions of why the return to the pinned structure occurs when (a) $T^* \approx T_c$ or else when (b) $F \approx F_0/2$.

First note that the fluid $\rightarrow c(2 \times 2)$ transition at $F = F_1$ is a nucleation phenomenon. This result is plausible since the sliding friction and the effective adsorbate temperature in Figs. 6(b) and 9 exhibit hysteresis and discontinuities as indeed expected for a nucleation process but a more direct proof is presented below. Assume now that the adsorbate structure is in a fluidized state ($F > F_1$) with the effective temperature T^* , which is higher than the substrate temperature T . If owing to a thermal fluctuation, an island of $c(2 \times 2)$ structure is temporarily formed in the fluid, the temperature in the island will in general be nonuniform in space and time. But if the island is large and if it survives for a long enough time the central region of the island would have a temperature close to the substrate temperature T while the tempera-

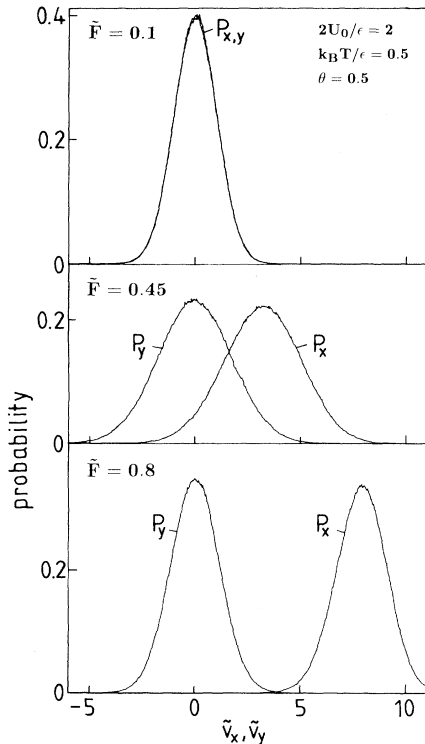


FIG. 10. The probability distributions P_x and P_y of adsorbate velocities for $\bar{F}=0.1, 0.45, 0.8$ and for $\theta=0.5$, $2U_0/\epsilon=2$, and $k_B T/\epsilon=0.5$. Both $P_x(v_x)$ and $P_y(v_y)$ are perfect Maxwellians of equal width.

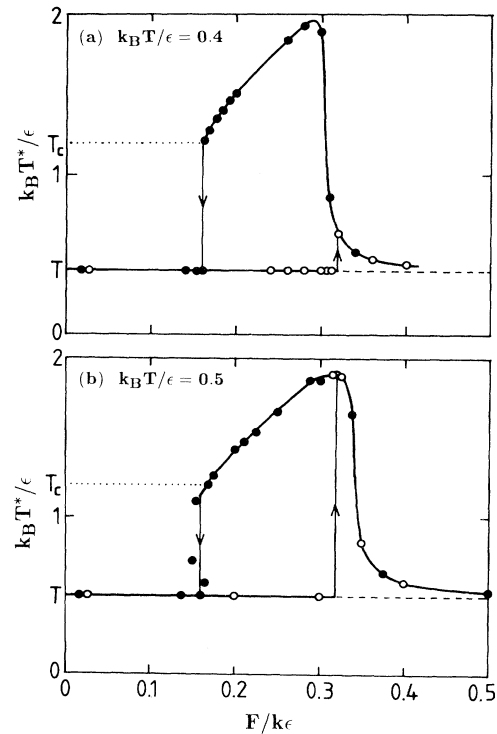


FIG. 11. The effective temperature T^* in the overlayer in units of ϵ , as a function of the force F in units of $k\epsilon$. In the calculations $2U_0/\epsilon=2$ and in (a) $k_B T/\epsilon=0.4$ while in (b) $k_B T/\epsilon=0.5$.

ture would be higher at the periphery of the cluster. The latter follows while the periphery of the cluster is in thermal contact to the surrounding fluid at temperature $T^* > T$. But if the heat transfer rate from the periphery to the central part of the island occurs slowly, or if the island is large enough, the central region would tend to be at a temperature only slightly above that of the substrate. It follows that the force *per adsorbate* necessary to fluidize a *very large* island equals F_0 , while the force is lower for a small island.

Next, note that the force which act on an adsorbate in an island has *two* contributions, namely, the external force \mathbf{F} plus a contribution from the *drag-force* \mathbf{F}_{drag} which act on the island from the surrounding flowing fluid. For a spherical object in a three-dimensional fluid this force (to first order in $v_0 R / \nu$) is given by Stokes formula. As shown in Appendix B, the drag force on a *large* rigid circular disk (radius R) in a two-dimensional fluid is given by $\mathbf{F}_{\text{drag}} = n_a \pi R^2 m \bar{\eta} \langle \mathbf{v} \rangle$, where $\langle \mathbf{v} \rangle$ is the drift velocity of the fluid far away from the disk. But since $n_a \pi R^2 = N$ is the number of adsorbates in the island and since $m \bar{\eta} \langle \mathbf{v} \rangle = \mathbf{F}$ we get $\mathbf{F}_{\text{drag}} = N\mathbf{F}$. Hence, the drag force *per adsorbate in the island is just \mathbf{F}* , and the total force *per adsorbate equals $2\mathbf{F}$* . This result is valid for a very large island; for a smaller island the drag force per adsorbate is even larger. It follows that if an island of $c(2 \times 2)$ structure is formed when $F > F_0/2$ it will “immediately” fluidize since the effective force on an adsorbate in the island equals $2F > F_0$ which is above the fluidization threshold of the $c(2 \times 2)$ structure. But if $F < F_0/2$, the total force $2F < F_0$, and if the island is large the drag force will not fluidize it. Hence, if the adsorbate temperature T^* is below T_c when $F = F_0/2$, one expects the fluid $\rightarrow c(2 \times 2)$ transition to occur at $F_1 = F_0/2$. But if the temperature T^* in the adsorbate layer (when $F = F_0/2$) is above the melting temperature T_c of the $c(2 \times 2)$ structure, then an island of $c(2 \times 2)$ structure would “immediately” melt. Hence, the return to the pinned structure in this latter case is expected to occur when $F = F_1 < F_0/2$ where $T^*(F_1) = T_c$. The discussion above assumes implicitly that the pinned island has a circular shape and that the drag force acts uniformly on all the adsorbates in the island.

One can argue that in most practical sliding systems the condition $T^* < T_c$ is satisfied. Hence, as shown above, the ratio F_1/F_0 between the kinetic and the static

friction force equals $\frac{1}{2}$. From this result one would also expect that the ratio f_k/f_s between the kinetic and the static friction coefficients should be approximately equal to $\frac{1}{2}$ for lubricated surfaces. That this is often the case is shown in Table I. Note that while f_s and f_k vary strongly between the different systems (by a factor of ~ 20) the ratio f_k/f_s is always close to 0.5. In fact, this ratio is nearly equal to 0.5 also for many “clean” surfaces. But note that “clean” surfaces, unless special care is taken, are covered by a layer of “grease” (hydrocarbons) which may have a very similar influence on the sliding friction as the lubricants quoted in Table I. In some cases the lubrication molecules may react so strongly with the surfaces that no fluidization of the adsorbate structures can occur; in this case there is no reason for why the ratio f_k/f_s should equal $\frac{1}{2}$. (This may be the case, for example, for fatty acids which are often used in boundary lubrication, see below.) But for the systems quoted in Table I this is certainly not the case; the interaction between the oil molecules (hydrocarbons) and the surfaces is mainly of van der Waals nature and weak.

It is interesting to note that (in accordance with theory) there is no correlation between the viscosity of a lubrication oil and the friction coefficients f_s and f_k and, in particular, the ratio $f_k/f_s \approx 0.5$ is independent of the film viscosity. For example, the oils in Table I have the following viscosities (in poises): Atlantic spindle oil, 0.33; Liberty aero oil, 8.92; castor oil, 4.73 but f_k and f_s are very similar in all cases. The ratio f_k/f_s averaged over all 12 measurements reported in Ref. 25 equals 0.51 ± 0.14 in good agreement with theory.

As pointed out above, the ratio f_k/f_s is expected to equal 0.5 only if sliding occurs via a set of fluidization \leftrightarrow solidification transitions which require that the adsorbate-substrate interaction potential is weakly corrugated. If this condition is not satisfied there is no reason for f_k/f_s to equal 0.5. This is illustrated in Table II for a number of sliding systems. The first few systems in Table II are inorganic layered lattice systems (similar to graphite). For these systems, as suggested by Bragg, the lubricity is due to the sliding of one lamella over another, which is made possible by the strong bonding forces within the planes and the relative weak bonding forces between the planes. The last four systems in Table II are fatty acids. These molecules have a polar “head” which is known to bind strongly to many metal oxides,

TABLE I. The static f_s and the kinetic f_k friction coefficient for a number of sliding systems. *a*, from Ref. 25; *b*, from Ref. 28; *c*, from Ref. 29; *d*, from Ref. 30. For the steel-on-ice system, a layer of water molecules will act as the lubricant during sliding.

System	Lubricant	f_s	f_k	f_k/f_s
steel on babbitt ^a	Atlantic spindle oil	0.25	0.13	0.52
	castor oil	0.12	0.06	0.50
	lard oil	0.10	0.05	0.50
steel on ice ^b	no lubricant	0.027	0.014	0.52
steel on lead ^{a,c}	medium mineral oil	0.50	0.30	0.6
bronze on bronze ^b	not specified	0.11	0.06	0.55
steel on steel ^{a,d}	castor oil	0.15	0.08	0.53

TABLE II. The static f_s and kinetic f_k friction coefficient for a number of sliding systems. From Ref. 31.

System	Lubricant	f_s	f_k	f_k/f_s
steel on steel	molybdenum disulfide	0.053	0.050	0.94
	barium hydroxide	0.163	0.151	0.93
	silver iodide	0.245	0.231	0.94
	borox	0.226	0.210	0.93
	rottenstone	0.195	0.189	0.97
	vermiculite	0.167	0.160	0.96
	iron-manganese-phosphate layer	0.218	0.213	0.98
	diethylene glycol stearate	0.089	0.083	0.93
	calcium stearate	0.113	0.107	0.95
	aluminum stearate	0.113	0.107	0.95
	lithium-12-hydroxy stearate	0.218	0.211	0.97

and a hydrocarbon "tail" which points away from the surface. In this case the adsorbate-substrate interaction is so strong that no fluidization can occur during sliding and, as discussed by Tabor, sliding is likely to occur between the ends of the hydrocarbon tails.

I have shown above that for $\theta=0.5$, when the adsorbate system is in a fluidized state, the probability distributions for $\delta v_x = v_x - \langle v_x \rangle$ and v_y are perfect Maxwellians with equal width. Nevertheless, the adsorbate-substrate system is not in thermal equilibrium but rather in a steady state with the temperature T^* of the adsorbate system being higher than the substrate temperature T . The reason why thermal equilibrium occurs within the adsorbate system is related to the high adsorbate cover-

age and concordant strong adsorbate-adsorbate interaction which tend to "randomize" the adsorbate velocities. But at low adsorbate coverages thermal equilibrium does not occur within the adsorbate layer. This is illustrated in Figs. 12 and 13 which show the velocity distributions P_x and P_y for $\theta=0.25$ and 0.01, respectively. In the latter case only one adsorbate occurs in the basic unit and the adsorbate-adsorbate interaction is negligible. Now, in this case P_y is a perfect Maxwellian with the width determined by the substrate temperature T . This result is expected since the adsorbate-substrate potential $u(r)$ is separable so that the motion in the y direction is independent of that in the x direction; hence the y motion does not depend on the external force F and the distribution

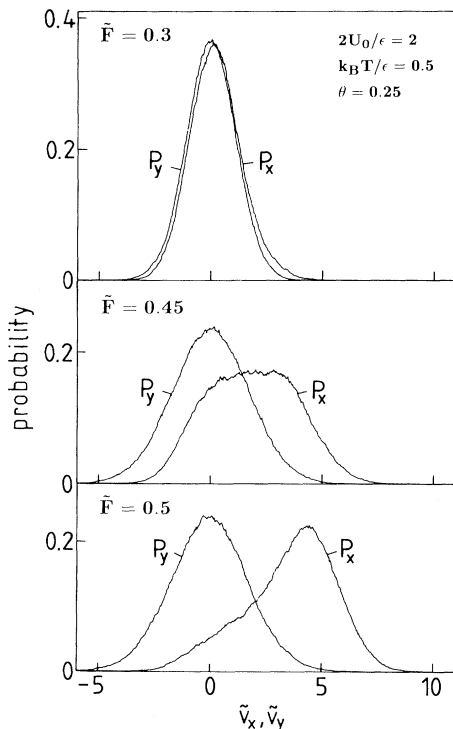


FIG. 12. The probability distributions P_x and P_y of adsorbate velocities for $\theta=0.25$, $2U_0/\epsilon=2$, and $k_B T/\epsilon=0.5$, and for $\tilde{F}=0.3, 0.45$, and 0.5.

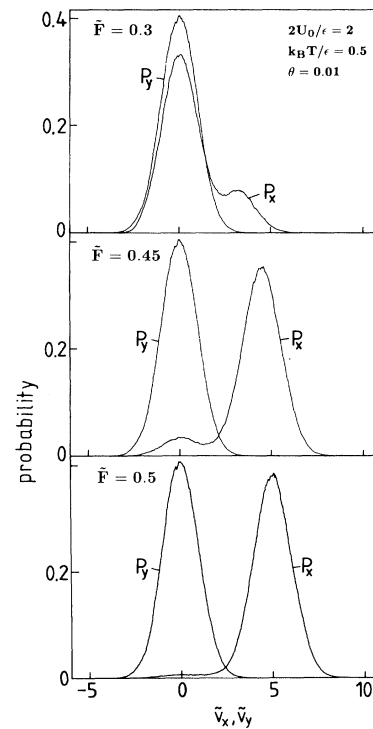


FIG. 13. The probability distributions P_x and P_y of adsorbate velocities for $\theta=0.01$, $2U_0/\epsilon=2$, and $k_B T/\epsilon=0.5$, and for $\tilde{F}=0.3, 0.45$, and 0.5.

P_y will be a Maxwellian with the width determined by the substrate temperature T . But this is not the case for P_x which exhibit a double-peak structure, see Fig. 13. The peak on the left-hand side is centered at $v_x=0$ and corresponds to adsorbate vibrations in the substrate potential wells. The peak on the right-hand side (RHS) corresponds to “fast” drift motion between (or over) the wells; in the present case where the friction η is small, once an adsorbate is thermally excited over a substrate barrier, it typically moves several lattice spacings before falling down in a new potential well. Note that the peak on the RHS is centered at a velocity v_x larger than $\langle v_x \rangle$, since in order for the net drift velocity to be $\langle v_x \rangle$ the adsorbates must drift faster than $\langle v_x \rangle$ during the time periods spent over the barriers to compensate for the time periods that they are trapped in the potential wells.

In Fig. 12, I show the velocity distributions P_x and P_y for $\theta=0.25$. In this case P_y is rather well described by a Maxwellian distribution. But P_x is strongly non-Maxwellian, i.e., the adsorbate-adsorbate interaction is not strong enough to “thermalize” the energy input from the external force F . In Fig. 14, I show for 0.25 the kinetic energy $m \langle (\delta v)^2 \rangle / 2$ in units of $k_B T$. If the adsorbate system were in thermal equilibrium this quantity would equal T^*/T as in Fig. 9, but we have seen above that this is not the case.

Let us compare the results presented above with the measurements of Israelachvili and co-workers.³ They have presented an extensive study of the sliding of two mica surfaces separated by a thin layer of a liquid (the lubricant). By varying the normal load they could change the separation d between the mica surfaces; this distance is known to within $\sim 1 \text{ \AA}$ from recording the optical fringe pattern from the sliding junction. Hence, the sliding friction can be measured as a function of the number of intervening layers n of lubricant molecules starting from $n=1$. As an example, in Fig. 15, I have reproduced their result for sliding with two layers ($n=2$) of octamethylcyclotetrasiloxane which is a nearly spherical molecule with diameter $\sim 8.5 \text{ \AA}$. The figure shows the

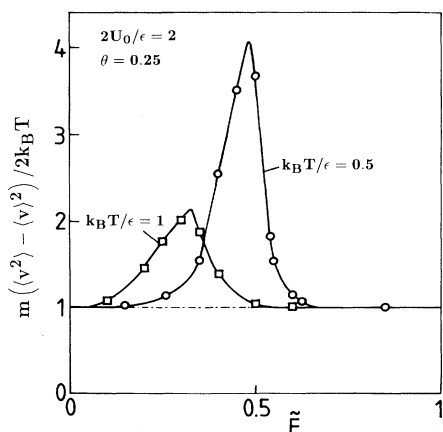


FIG. 14. The kinetic energy $m \langle \delta v^2 \rangle / 2$ in units of $k_B T$. The circles and squares show results for $k_B T / \epsilon = 0.5$ and 1.0, respectively. In the calculations $2U_0 / \epsilon = 2$ and $\theta = 0.25$.

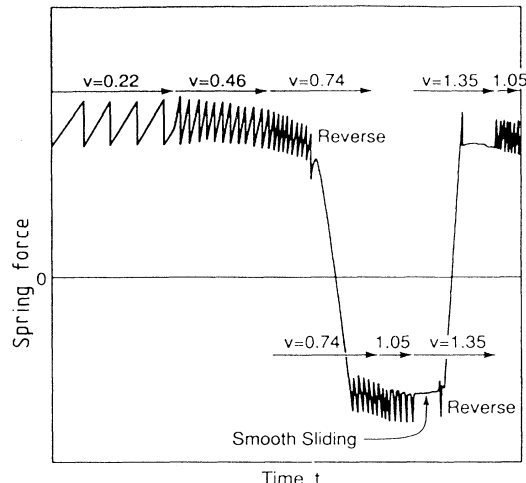


FIG. 15. Effect of increasing the velocity v on the spring force of a two-layer film of octamethylcyclotetrasiloxane. On increasing v from 0.22 to 1.05 $\mu\text{m/s}$ the stick-slip frequency increases while the stick-slip amplitude ΔF fall, but only slightly. However, once v exceeds the critical velocity v_c (between 1.05 and 1.35 $\mu\text{m/s}$) the stick-slip disappears abruptly, and returns equally abruptly when v falls below v_c again. From Ref. 3.

spring force as a function of the velocity v (in units of $\mu\text{m/s}$) of the free end of the spring. As v increases, the stick time decreases while the amplitude ΔF of the oscillations in the spring force is nearly constant until v reaches a critical spread v_c where stick-slip suddenly disappear ($\Delta F=0$) and is replaced by smooth sliding. The disappearance of stick-slip for $v > v_c$ must, as has been pointed out by Israelachvili and co-workers, be due to “slow” molecular relaxation processes in the lubrication film. More generally, Gee, McGuiggan, and Israelachvili found that the stick-slip was very sensitive not only to the sliding velocity but also to the immediately previous history of sliding. For example, if smooth sliding (i.e., $v > v_c$) is suddenly stopped and then restarted, it was found that if the stopping time is less than a certain time τ^* there is no change in the friction on restarting, i.e., the sliding proceeds as if there had been no interruption. But if the resting time exceeds τ^* a single fully developed stick-slip spike occurs. This indicates that well after the surface have stopped moving relative to each other, the molecules in the gap are still relaxing and that some dramatic change in their configuration occurs at time τ^* after stopping. Furthermore, the fact that the stick-slip spikes occur very abruptly for $t > \tau^*$ indicates that the molecular relaxations in the resting regime may be a nucleation phenomenon rather than a continuous process. Experiments with several kinds of liquids have shown that τ^* is longer for more complex branched chain molecules as compared with smaller nearly spherical molecules; this result is expected as the former molecules need more time to “disentangle” and relax to the local minima in the adsorbate-substrate potential.

In light of the simulations presented above, these interesting effects in the sliding experiments are not unex-

pected: During sliding the adsorbate system is in a “fluidized” state, see Fig. 7(b). If the external force F is suddenly reduced below F_1 it takes some time τ^* (depending on the final force) for the fluid overlayer to relax to the minimum free-energy configuration shown in Fig. 7(a). This is illustrated in Fig. 16(a) which shows the time variation of the center-of-mass velocity $\bar{v}(t)$ as the external force is changed from $\bar{F}=0.4 > \bar{F}_1$ to $0.2 < \bar{F}_1$ at $t=1500\tau \equiv t_1$. For $t < t_1$ the system is in a fluidlike state and the drift friction $\eta/\bar{\eta} \approx 0.6$ as in Fig. 6. For $t > t_1$ the stable state is the pinned $c(2 \times 2)$ structure, see *C* in Fig. 17, for which the drift velocity vanishes. But Fig. 16(a) shows that the system does not immediately switch to this configuration at $t=t_1$ but remains in a fluidlike configuration (see *B* in Fig. 17) until $t_1 + \tau^*$ ($\tau^* \approx 750\tau$), where it suddenly jumps to the $c(2 \times 2)$ structure. The abruptness of the transition indicates a nucleation phenomena, i.e., the $c(2 \times 2)$ phase is nucleating in the fluidlike phase. That this is indeed the case was proved by performing very many simulations with slightly different times for the switching $\bar{F}=0.4 \rightarrow 0.2$ —see Fig. 18 for

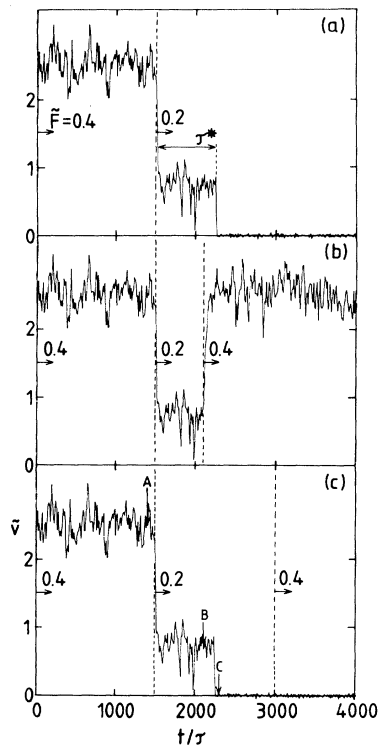


FIG. 16. (a) The velocity of the center of mass of the adsorbate system as a function of time (more precisely, the velocity in the x direction averaged over all the adsorbates and over a short time interval, 10τ). Initially, up to $t=1500\tau$, the velocity is so large $\bar{F}=0.4$ that the “fluid” state is stable and the drift velocity is high. At $t=1500\tau$ the external force is instantaneously reduced to $\bar{F}=0.2$. The system remains in a metastable fluidlike state for a time τ^* before returning to the pinned $c(2 \times 2)$ state. (b) The same as (a) except that the force \bar{F} is switched back to 0.4 at $t=2100\tau$. (c) The same as (a) except that the force is switched back to 0.4 at $t=3000\tau$. In the simulations $2U_0/\epsilon=2$, $k_B T/\epsilon=0.5$, and $\eta\tau=0.1$.

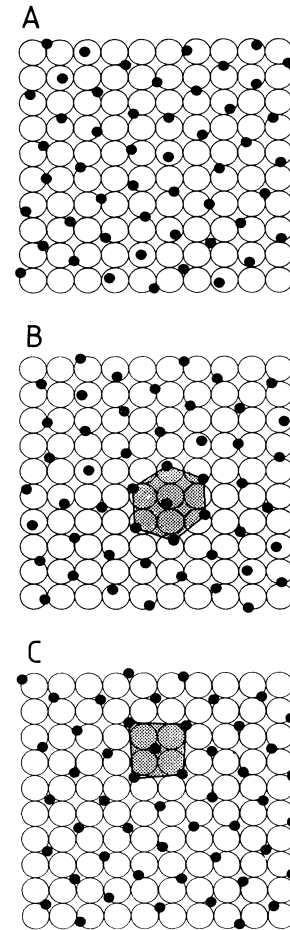


FIG. 17. Snapshot pictures of the adsorbate structure at time points *A* ($t=1400\tau$), *B* ($t=2100\tau$), and *C* ($t=2300\tau$) indicated in Fig. 16(c).

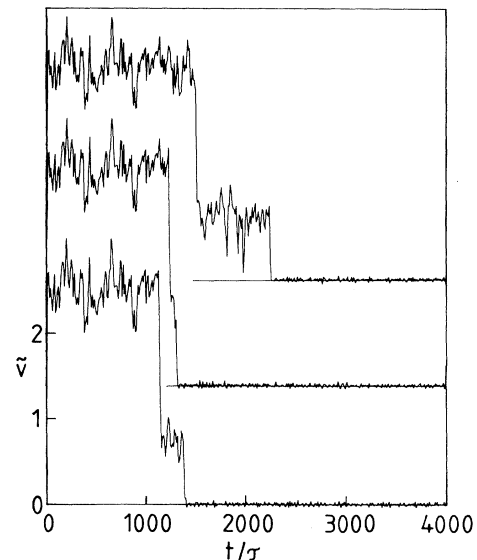


FIG. 18. The velocity \bar{v} (see Fig. 16 for the definition) as a function of time in three different cases. Initially, the external force $\bar{F}=0.4$, but at three different time points the force is instantaneously reduced to $\bar{F}=0.2$.

three examples. In all cases the velocity \bar{v} in the intermediate state had the same value (when averaged over the thermal noise) but the duration τ^* of this time period varied randomly between the different cases, with a width of the probability distribution $P(\tau^*)$ being of similar magnitude as the mean time $\langle \tau^* \rangle$, as indeed expected for a nucleation type of phase transition. Furthermore, as is illustrated in Figs. 16(b) and 16(c), the system exhibits memory effects similar to those observed by Gee, McGuiggan, and Israelachvili. Figure 16(b) shows the same simulation as in 16(a), except that the force \bar{F} is switched back to 0.4 at $t_2 < t_1 + \tau^*$. In this case the sliding velocity returns to the value it had for $t < t_1$, i.e., the system “remembers” its original sliding state. However, if $t_2 > t_1 + \tau^*$, the system remains in the pinned state even if \bar{F} is increased to 0.4, see Fig. 16(c). The relaxation time τ^* depends sensitively on the adsorbate-substrate and the adsorbate-adsorbate interactions and can vary from nanoseconds to seconds or more, if the barriers involved in the molecular reorganization processes are large.

It is interesting to note that the snapshot picture in *B* in Fig. 17 shows a high degree of short-ranged order—a triangular structure tends to be formed—while that in *A* in Fig. 17 is more disordered. We can explain this with the relation between the external force F and effective temperature T^* in the adsorbate layer shown in Fig. 9: As F increases (but $\bar{F} < 0.6$) the effective temperature T^* increases and the system becomes more and more disordered.

At this point, let me comment on the molecular dynamics simulations of Thompson and Robbins. They studied relative thick ($d \sim 11r_0$) fluid layers between two parallel solid slabs. A spring was attached to the “top” slab and the free end of the spring moved with the constant velocity v . In the simulations, the top slab did not move until the spring force reached some critical value F_0 . For low spring velocity v , stick-and-slip motion was observed. When v increased further smooth sliding finally occurred. Thompson and Robbins argued that the solid, static slabs induce crystalline order in the film and that during the stick-and-slip motion periodic shear-melting transitions and recrystallization of the film occur. Uniform motion occurred at high sliding velocity where the film no longer had time to order. These results are similar to those observed above in our simulations if a solid adsorbate structure occurred when $F = 0$.

In most of the simulations presented above, only the *steady-state* properties of the adsorbate system where probed but by applying an oscillating (in time) external force it is possible to probe the nonlocal (in time) drift friction which is needed in order to study the sliding friction in the most general case. Note, however, that because of the long relaxation times ($\tau^* \sim 1$ s) involved in many “real” systems, it may, in general, be hard to study this relaxation process directly via computer simulations.

In the simulations presented above the substrate is perfectly periodic and a unique (ordered) adsorbate structure could be easily formed. Many real surfaces are much more complicated with impurities (pinning centers) and no periodic adsorbate structure will occur. Nevertheless

even in these cases one may, in general, expect the sliding friction to exhibit hysteresis if solid adsorbate structures can be formed, since when the sliding has stopped the adsorbates will relax from the “fluidized” sliding configuration to some (nonperiodic) structure which corresponds to a minima of the free energy. Of course, in this case a large number of almost degenerate local energy minima may occur in configuration space and the system will in general not have enough time to find the absolute minima. This situation is similar to the spin-glass problem where “memory effects” and a wide distribution of relaxation times occurs.

It is interesting to note that in “normal” liquids typical relaxation times are of order picoseconds, or so, while the molecular rearrangement processes observed by Gee, McGuiggan, and Israelachvili occur on the scale of seconds. The fundamental difference is the large (on the scale of the thermal energy $k_B T \sim 25$ meV) diffusion or rearrangement barriers which often occur for adsorbed molecules but which are absent in liquids. These barriers are particularly large for adsorbates on nonmetals, where relative localized bonds may have to be broken and reformed as an adsorbate moves parallel to the substrate. This is also true for mica surfaces which has a large unit cell, with well-separated bonding sites, which may give rise to a relatively strongly corrugated substrate potential (see below).

In this context it is interesting to note that a drastic reduction (typically by a factor of $\frac{1}{100}$) in the sliding friction (and the absence of “stick-and-slip”) occurs if water is introduced in the lubricant.³ Now, it is known that water binds very strongly to mica surfaces, and the water molecules in the lubricant will migrate to the mica surfaces where it forms overlayers. The sliding will now almost certainly occur between the water layers and the lubricant layer and *if* the barrier towards the lateral motion of the lubricant molecules is much smaller for a water-converged surface than for the clean surface, this leads to a drastically reduced sliding friction. Now, a clean mica surface has a large unit cell and the surface is strongly polar. Hence, even for a saturated hydrocarbon molecule, where no direct “chemistry” is expected to be involved in the adsorbate-substrate bond, a relative large lateral corrugation in the binding potential is expected because of electrostatic interactions between the adsorbate and the polar groups on the mica surface (the charges on the mica surface induces dipoles in the adsorbates giving rise to charge-induced dipole interactions). But the electric field from the polar groups on the mica surface will be almost completely screened out when a layer of water molecules occurs on the mica surface. This results in a much weaker corrugated interaction potential between the lubrication molecules and the mica surfaces and hence to a strongly reduced sliding friction.

The measurements of Gee, McGuiggan, and Israelachvili were performed on extremely smooth mica surfaces and the observed “stick-and-slip” motion is likely to involve the whole contact area simultaneously. However, most “practical” sliding systems involve surfaces which are relative “rough,” at least on the microscopic scale. Hence it is very likely that different surface areas in the

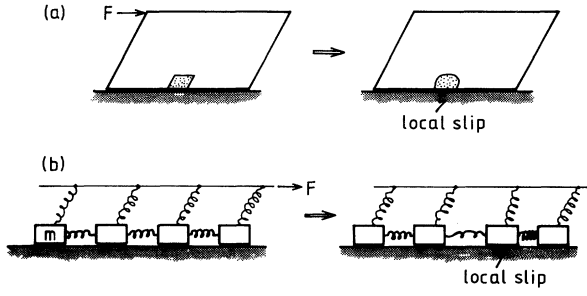


FIG. 19. (a) An elastic block on a substrate. Left: the force F deforms the block elastically but the surface stress $F/\delta A$ (where δA is the contact area) is below the minimum critical stress σ_0 necessary for a local sliding to occur. Right: $F/\delta A > \sigma_0$ and the area under the dotted volume element have undergone sliding. The local stress at the slid area equals $\sigma_1 < \sigma_0$. (b) A simple model which allows one to study the cooperative nature of the sliding process.

contact region experience different pinning potentials, i.e., the local surface stress σ_0 , which must be overcome for sliding to occur, vary over the surface. The consequences this has on the sliding process are illustrated in Fig. 19. Here a solid block slides on a surface and it is assumed that the critical surface stress σ_0 has its smallest value on the surface area ΔA , where the dotted volume element in Fig. 19 is in contact with the substrate. Hence, as the force F increases, when the surface stress $F/\delta A$ reaches the value σ_0 the local surface area ΔA will slide and stop first when the local surface stress falls below the kinetic sliding stress σ_1 . In Fig. 19(a) this local relaxation of the elastic body is indicated by the change in the shape of the dotted volume element before and after sliding. Since the local stress at the slid surface area ΔA is lower than σ_0 , it follows that the surface stress on the unslid surface area is higher after sliding than before. For a macroscopic solid block, where one may assume the existence of an almost continuous distribution of local critical stresses σ_0 , it follows that the initial sliding may initiate further sliding on other surface areas. This in turn increases the surface stress even further on the surface area which has not undergone sliding. This may result in an increasing number of local sliding events which could end up with the whole surface moving relative to the substrate.

The simple model presented in Fig. 19(b) may be used to gain further insight into the nature of this collective sliding processes. This model is similar to the one studied by Carlson and Langer²⁶ in the context of earthquakes, with the modification that a distribution of critical stresses σ_0 and σ_1 now occur.

VI. SUMMARY

The most important results of this study can be summarized as follows.

(a) I have studied the coverage and temperature dependence of the linear sliding friction for adsorbates on a (100) surface of a fcc crystal. These simulations were

based on Langevin dynamics and were performed on systems with both “small” and “large” corrugation of the adsorbate-substrate interaction potential and with Lennard-Jones interaction potentials between the particles. In the former case the sliding velocity increases monotonically with increasing coverage, while in the latter case (at low enough temperature) an ordered commensurate structure is formed at the coverage $\theta=0.5$, where the drift velocity is extremely small.

(b) I have studied the nonlinear sliding friction and shown that for solid adsorbate structures the relation $\langle v \rangle = f(F)$ between the drift velocity $\langle v \rangle$ and the external force F exhibit hysteresis which implies “stick-and-slip” motion for macroscopic bodies. For liquid overlayers no hysteresis occurs which implies smooth sliding.

(c) I have shown that if the adsorbate layer is in a solid phase the ratio F_1/F_0 between the kinetic and the static friction force equals $\frac{1}{2}$ for a large class of sliding systems. This is in good agreement with experimental data for the ratio f_k/f_s between the kinetic and the static friction coefficient.

ACKNOWLEDGMENTS

I thank Uzi Landman for many interesting discussions related to friction.

APPENDIX A

In this appendix, I study the sliding motion of adsorbate systems when the external force $\mathbf{F}=F\hat{x}$ is very strong. We have

$$m\ddot{\mathbf{r}}_i + m\eta\dot{\mathbf{r}}_i = -\frac{\partial U}{\partial \mathbf{r}_i} - \frac{\partial V}{\partial \mathbf{r}_i} + \mathbf{F} + \mathbf{f}_i. \quad (\text{A1})$$

Let us write

$$\mathbf{r}_i = \mathbf{v}_0 t + \mathbf{x}_i, \quad (\text{A2})$$

where

$$m\eta\mathbf{v}_0 = \mathbf{F}. \quad (\text{A3})$$

Substituting (A2) into (A1) gives

$$m\ddot{\mathbf{x}}_i + m\eta\dot{\mathbf{x}}_i = -\frac{\partial U}{\partial \mathbf{x}_i} - \frac{\partial V}{\partial \mathbf{x}_i} + \mathbf{f}_i, \quad (\text{A4})$$

where

$$U(\mathbf{x}_i) = U_0[2 - \cos k(v_0 t + x_i) - \cos ky_i].$$

Note that V is independent of time. The x component of (A4) gives

$$m\ddot{x}_i + m\eta\dot{x}_i = -kU_0 \sin(\omega t + kx_i) - \frac{\partial V}{\partial x_i} + f_{xi}, \quad (\text{A5})$$

where $\omega = kv_0$. Let us write

$$x_i = X_i + \xi_i, \quad (\text{A6})$$

where X_i and ξ_i vary “slowly” and “fast” with time, respectively.

Now, let us choose ξ_i to satisfy

$$m\ddot{\xi}_i + m\eta\dot{\xi}_i = -kU_0 \sin(\omega t + kX_i). \quad (\text{A7})$$

Since X_i varies slowly with time, we get

$$\dot{\xi}_i \approx \frac{kU_0}{2mi} \left[\frac{e^{i(\omega t + kX_i)}}{\omega^2 - i\omega\eta} - \frac{e^{-i(\omega t + kX_i)}}{\omega^2 + i\omega\eta} \right]. \quad (\text{A8})$$

Using (A5)–(A7) gives

$$m\ddot{X}_i + m\eta\dot{X}_i = -kU_0 [\sin(\omega t + kX_i + k\xi_i) - \sin(\omega t + kX_i)] - \frac{\partial V}{\partial x_i} + f_{xi}.$$

Expanding to first order in ξ_i and averaging (denoted by an overbar) over the time period $T=2\pi/\omega$ gives

$$m\ddot{X}_i + m\eta\dot{X}_i = -k^2 U_0 \overline{\xi_i \cos(\omega t + kX_i)} - \frac{\partial V}{\partial x_i} + f_{xi}. \quad (\text{A9})$$

Next, using (A8),

$$\begin{aligned} \overline{\xi_i \cos(\omega t + kX_i)} &= \frac{kU_0}{2m} \frac{\omega\eta}{\omega^4 + \omega^2\eta^2} \\ &\approx \frac{kU_0}{2m} \frac{\eta}{\omega^3} \end{aligned} \quad (\text{A10})$$

since $\omega \gg \eta$ when F is “large.” Substituting (A10) into (A9) gives

$$m\ddot{X}_i + m\eta\dot{X}_i = -\frac{k^3 U_0^2}{2m} \frac{\eta}{\omega^3} - \frac{\partial V}{\partial x_i} + f_{xi}. \quad (\text{A11})$$

Hence, integrating out the rapid motion results in an effective equation of motion for $x_i(t)$ where the periodic force associated with the corrugated substrate potential is replaced by a constant force. Using (A2) and (A11), we obtain the drift velocity

$$\langle v \rangle = v_0 - \frac{k^3 U_0^2}{2m^2} \frac{1}{\omega^3}.$$

But $m\bar{\eta}\langle v \rangle = m\eta v_0 = F$ so that

$$\frac{\eta}{\bar{\eta}} = 1 - \frac{k^3 U_0^2}{2mF} \frac{\eta}{\omega^3}.$$

Substituting $\omega = kv_0 = kF/m\eta$ in this equation gives

$$\frac{\eta}{\bar{\eta}} = 1 - \frac{1}{2} U_0^2 m^2 \left[\frac{\eta}{F} \right]^4. \quad (\text{A12})$$

This formula is valid only if the last term is much smaller than unity, i.e., $F \gg (mU_0)^{1/2}\eta$. Note that if we introduce $K = mv_0^2/2$, which is the drift kinetic energy an ad-

sorbate would have if the surface were perfectly flat (i.e., $U_0=0$), then (A12) can be written as

$$\langle v \rangle = v_0 \left[1 - \frac{U_0^2}{8K^2} \right].$$

This formula is valid only if $K \gg U_0$, i.e., the drift kinetic energy must be much larger than the substrate corrugation U_0 .

APPENDIX B

In this appendix, I derive an expression for the drag force on a stationary circular disk (radius R) in a two-dimensional fluid. The external force \mathbf{F} acts on each fluid atom and, far away from the disk, gives rise to the drift velocity \mathbf{v}_0 where $m\bar{\eta}\mathbf{v}_0 = \mathbf{F}$. The basis equations are

$$\nabla \cdot \mathbf{v} = 0, \quad (\text{B1})$$

$$\frac{\partial \mathbf{v}}{\partial t} + \mathbf{v} \cdot \nabla \mathbf{v} = -\frac{1}{mn_0} \nabla p + \nu \nabla^2 \mathbf{v} - \bar{\eta}(\mathbf{v} - \mathbf{v}_0). \quad (\text{B2a})$$

If we measure velocity in units of v_0 and distance in units of R then the terms

$$\mathbf{v} \cdot \nabla \mathbf{v}: \nu \nabla^2 \mathbf{v}: \bar{\eta} \mathbf{v}$$

will scale as

$$v_0^2/R: \nu v_0/R^2: \bar{\eta} v_0$$

or

$$v_0 R/\nu: 1: R^2 \bar{\eta}/\nu.$$

Hence, the large- and small- R limits will be correct even if we drop the nonlinear term $\mathbf{v} \cdot \nabla \mathbf{v}$ (see discussion below, however). If, in addition, we consider stationary flow, $\partial \mathbf{v}/\partial t = 0$, then (B2a) reduces to

$$-\frac{1}{mn_0} \nabla p + \nu \nabla^2 \mathbf{v} - \bar{\eta}(\mathbf{v} - \mathbf{v}_0) = 0. \quad (\text{B2b})$$

The drag force is given by

$$(\mathbf{F}_{\text{drag}})_i = \oint d\varphi [-px_i + mn_0 \nu (v_{i,j} + v_{j,i}) x_j], \quad (\text{B3})$$

where the integral is over the periphery of the disk, i.e., $|\mathbf{x}|=R$ and $0 \leq \varphi < 2\pi$. Let \mathbf{n} be a unit vector normal to the xy plane occupied by the fluid. Let us write

$$\mathbf{v} = \nabla A + \mathbf{n} \times \nabla B + \mathbf{v}_0. \quad (\text{B4})$$

Now, note that

$$x_j (v_{i,j} + v_{j,i}) = \mathbf{x} \cdot \nabla v_i + (v_j x_j)_i - v_i. \quad (\text{B5})$$

Substituting (B4) into (B5) gives

$$\mathbf{x} \cdot \nabla (\nabla A + \mathbf{n} \times \nabla B) + \nabla (\mathbf{x} \cdot \nabla A + \mathbf{x} \cdot \mathbf{n} \times \nabla B) - \nabla A - \mathbf{n} \times \nabla B = \mathbf{x} \cdot \nabla (2\nabla A + \mathbf{n} \times \nabla B) + \mathbf{x} \times \mathbf{n} \cdot \nabla \nabla B. \quad (\text{B6})$$

But note that $\mathbf{x} \times \mathbf{n} \cdot \nabla = -\partial/\partial\varphi$, where (r, φ) are polar coordinates. Hence the last term in (B6) does not contribute to the integral in (B3). Thus, using (B3) and (B6),

$$\mathbf{F}_{\text{drag}} = \oint d\varphi [-p\mathbf{x} + mn_0 v\mathbf{x} \cdot \nabla (2\nabla A + \mathbf{n} \times \nabla B)]. \quad (\text{B7})$$

Next, substituting (B4) into (B1) gives

$$\nabla^2 A = 0. \quad (\text{B8})$$

Substituting (B4) into (B2b) and using (B8) gives

$$-\frac{1}{mn_0} \nabla p + v\mathbf{n} \times \nabla \nabla^2 B - \bar{\eta} \nabla A - \bar{\eta} \mathbf{n} \times \nabla B = 0. \quad (\text{B9})$$

Operating with $\nabla \cdot$ on this equation and using (B8) gives

$$\nabla^2 p = 0. \quad (\text{B10})$$

Next, operating with $\mathbf{n} \times \nabla \cdot$ on (B9) gives

$$\nabla^2 (v \nabla^2 B - \bar{\eta} B) = 0. \quad (\text{B11})$$

$$-\frac{1}{mn_0} \left[\frac{\mathbf{b}}{r^2} - \frac{2\mathbf{b} \cdot \mathbf{xx}}{r^4} \right] - \bar{\eta} \left[\frac{\mathbf{a}}{r^2} - \frac{2\mathbf{a} \cdot \mathbf{xx}}{r^4} \right] - \bar{\eta} \mathbf{n} \times \left[\frac{\mathbf{c}}{r^2} - \frac{2\mathbf{c} \cdot \mathbf{xx}}{r^4} \right] = 0. \quad (\text{B17})$$

Hence

$$\mathbf{b} = -mn_0 \bar{\eta} \mathbf{a}, \quad \mathbf{c} = 0.$$

Substituting these results in (B13) and (B14) gives

$$p = -mn_0 \bar{\eta} \mathbf{a} \cdot \mathbf{x} / r^2, \quad (\text{B18})$$

$$B = \mathbf{d} \cdot \mathbf{x} f(r). \quad (\text{B19})$$

Substituting (B12), (B18), and (B19) into (B7) gives

$$\mathbf{F}_{\text{drag}} = mn_0 \pi \{ \bar{\eta} \mathbf{a} + v\mathbf{n} \times \mathbf{d} [2rf' + r(rf')']_{r=R} \}.$$

But from (B16)

$$v[2rf' + r(rf')'] = \bar{\eta} r^2 f.$$

Hence

$$\mathbf{F}_{\text{drag}} = mn_0 \pi \bar{\eta} (\mathbf{a} + \mathbf{n} \times \mathbf{d} R^2 f). \quad (\text{B20})$$

Next, assuming no slip at the periphery of the disk one gets $\mathbf{v} = 0$ for $r = R$. Hence, using (B4),

$$\mathbf{x} \cdot \mathbf{v} = \mathbf{x} \cdot \nabla A + \mathbf{x} \times \mathbf{n} \cdot \nabla B + \mathbf{x} \cdot \mathbf{v}_0 = 0,$$

$$\mathbf{n} \times \mathbf{x} \cdot \mathbf{v} = \mathbf{n} \times \mathbf{x} \cdot \nabla A + \mathbf{n} \times \mathbf{x} \cdot \mathbf{n} \times \nabla B + \mathbf{n} \times \mathbf{x} \cdot \mathbf{v}_0 = 0$$

for $r = R$, or since $\mathbf{n} \times \mathbf{x} \cdot \nabla = \partial/\partial\varphi$ and $\mathbf{n} \times \mathbf{x} \cdot \mathbf{n} \times \nabla = R \partial/\partial R$,

$$R \frac{\partial A}{\partial R} - \frac{\partial B}{\partial \varphi} + R v_0 \cos \varphi = 0, \quad (\text{B21})$$

$$\frac{\partial A}{\partial \varphi} + R \frac{\partial B}{\partial R} - R v_0 \sin \varphi = 0. \quad (\text{B22})$$

Now, in order to satisfy these boundary conditions, one

The relevant solutions of (B8) and (B10) are of the form

$$A = \mathbf{a} \cdot \mathbf{x} / r^2, \quad (\text{B12})$$

$$p = \mathbf{b} \cdot \mathbf{x} / r^2, \quad (\text{B13})$$

where \mathbf{a} and \mathbf{b} are two constant vectors. Next, the relevant solution of (B11) is of the form

$$B = \mathbf{c} \cdot \mathbf{x} / r^2 + \mathbf{d} \cdot \mathbf{x} f(r), \quad (\text{B14})$$

where

$$\left[\nabla^2 - \frac{\bar{\eta}}{v} \right] [\mathbf{d} \cdot \mathbf{x} f(r)] = 0 \quad (\text{B15})$$

or, in polar coordinates,

$$\frac{d^2}{dr^2} (rf) + \frac{1}{r} \frac{d}{dr} (rf) - \frac{1}{r^2} (rf) - \frac{\bar{\eta}}{v} (rf) = 0, \quad (\text{B16})$$

i.e., $rf = K_1(\alpha r)$ where $\alpha = (\bar{\eta}/v)^{1/2}$ and where K_1 is a modified Bessel function. Substituting (B12), (B13), and (B14) into (B9) gives

must take $\mathbf{a} \cdot \mathbf{x} = ar \cos \varphi$ and $\mathbf{d} \cdot \mathbf{x} = dr \sin \varphi$. Substituting (B12) and (B19) into (B21) and (B22) gives

$$a + dR^2 f(R) - R^2 v_0 = 0,$$

$$a - dR^2 [Rf(R)]' + R^2 v_0 = 0,$$

or

$$d = \frac{2v_0}{f(R) + [Rf(R)]'}.$$

Using these results in (B20) gives

$$\begin{aligned} \mathbf{F}_{\text{drag}} &= mn_0 \pi R^2 \bar{\eta} \frac{(Rf)' - 3f}{(Rf)' + f} \mathbf{v}_0 \\ &= mn_0 \pi R^2 \bar{\eta} \frac{\alpha R K_1'(\alpha R) - 3K_1(\alpha R)}{\alpha R K_1'(\alpha R) + K_1(\alpha R)} \mathbf{v}_0. \end{aligned}$$

But, since

$$K_1'(\alpha R) = -K_0(\alpha R) - K_1(\alpha R)/\alpha R,$$

we get

$$\mathbf{F}_{\text{drag}} = mn_0 \pi R^2 \bar{\eta} \left[1 + \frac{4}{\alpha R} \frac{K_1(\alpha R)}{K_0(\alpha R)} \right] \mathbf{v}_0. \quad (\text{B23})$$

Let us consider two limits of (B23). Since $K_1(\alpha R)/K_0(\alpha R) \rightarrow 1$ as $\alpha R \rightarrow \infty$, we get

$$\mathbf{F}_{\text{drag}} \sim mn_0 \pi R^2 \bar{\eta} \mathbf{v}_0 \quad (\text{B24})$$

as $\alpha R \rightarrow \infty$. Next, let $\alpha R \rightarrow 0$. Since $K_1(\alpha R) \sim 1/(\alpha R)$ and $K_0(\alpha R) \sim -\ln(\alpha R/2)$ as $\alpha R \rightarrow 0$, we get

$$\mathbf{F}_{\text{drag}} \sim \frac{4\pi mn_0 \nu}{-\ln(\alpha R/2)} \mathbf{v}_0 \quad (\text{B25})$$

as $\alpha R \rightarrow 0$.

Finally, let me add the following comment. Note first that according to (B25), $\mathbf{F}_{\text{drag}} \rightarrow 0$ as $\bar{\eta} \rightarrow 0$, which is an unphysical and incorrect result. To see this, suppose we put $\bar{\eta} = 0$ in (B2a) and for the moment neglect the complications that this has for the existence of two-dimensional hydrodynamics (e.g., the divergence of the physical "macroscopic" viscosity). It is well known that in this case it is necessary to keep the nonlinear term in (B2) when calculating the drag force on a circular disk; otherwise no solution satisfying the boundary condition $\mathbf{v} = 0$ at the periphery of the disk exists for the Navier-Stokes equations. As shown by Lamb,²⁷ to leading order in

$v_0 R / \nu$ one now has the same result as (B25) except that the argument of the logarithmic function in (B25) is replaced by $v_0 R / 4\nu$. Hence even when $\bar{\eta} \neq 0$ it is necessary to keep the nonlinear term $\mathbf{v} \cdot \nabla \mathbf{v}$ in (B2) in order to obtain the correct limiting formula as $R \rightarrow 0$. To leading order in αR and $v_0 R / \nu$ such a treatment gives

$$\mathbf{F}_{\text{drag}} \sim \frac{4\pi mn_0 \nu}{-\ln(qR/2)} \mathbf{v}_0, \quad (\text{B26})$$

where

$$q = \left[\frac{\bar{\eta}}{\nu} + \frac{v_0^2}{4\nu^2} \right]^{1/2}.$$

This formula reduces to (B25) if $v_0 R / \nu \rightarrow 0$ and to the other known limit as $\bar{\eta} \rightarrow 0$.

- ¹D. Tabor, in *Microscopic Aspects of Adhesion and Lubrication, Tribology Series 7*, edited by J. M. Georges (Elsevier, New York, 1982), pp. 651–682.
- ²F. P. Bowden and D. Tabor, *Friction and Lubrication* (Methuen, London, 1967), pp. 17 and 18; J. F. Archard, Proc. R. Soc. London Ser. A **243**, 190 (1957).
- ³M. L. Gee, P. M. McGuiggan, and J. N. Israelachvili, J. Chem. Phys. **93**, 1895 (1990).
- ⁴E. Rabinowicz, *Friction and Wear of Materials* (Wiley, New York, 1965).
- ⁵E. Rabinowicz and D. Tabor, Proc. R. Soc. London Ser. A **208**, 455 (1951).
- ⁶U. Landman, W. D. Luedtke, N. A. Burnham, and R. J. Colton, Science **248**, 454 (1990).
- ⁷J. N. Israelachvili, Surf. Sci. Rep. **14**, 109 (1992).
- ⁸M. L. Gee, P. M. McGuiggan, and J. N. Israelachvili, J. Chem. Phys. **93**, 1895 (1990).
- ⁹P. A. Thompson and M. O. Robbins, Phys. Rev. A **41**, 6830 (1990); Science **250**, 792 (1990).
- ¹⁰R. Erlandsson, G. Hadziioannou, C. M. Mate, G. M. McClelland, and S. Chiang, J. Chem. Phys. **89**, 5190 (1988); C. Mathew, Gary M. McClelland, R. Erlandsson, and S. Chiang, Phys. Rev. Lett. **59**, 1942 (1987).
- ¹¹E. Meyer, R. Overney, D. Brodbeck, L. Howald, R. Lüthi, J. Frommer, and H.-J. Güntherodt, Phys. Rev. Lett. **69**, 1777 (1992).
- ¹²B. N. J. Persson, in *Computations for the Nano-Scale* Vol. 240 of *NATO Advanced Study Institute Series E*, edited by P. E. Blöchl, C. Joachim, and A. J. Fisher (Kluwer, Dordrecht, 1993), p. 21.
- ¹³B. N. J. Persson, J. Chem. Phys. **98**, 1659 (1993).
- ¹⁴T. Schneider and E. Stoll, Phys. Rev. B **17**, 1302 (1978).
- ¹⁵See, e.g., Dieter Foster, *Hydrodynamic Fluctuations, Broken Symmetry, and Correlation Functions* (Benjamin, New York, 1975).
- ¹⁶J. Krim and R. Chiarello, J. Vac. Sci. Technol. A **9**, 2566 (1991).
- ¹⁷G. Wahnström, Surf. Sci. **159**, 311 (1985); Phys. Rev. B **33**, 1020 (1986).
- ¹⁸B. N. J. Persson and R. Ryberg, Phys. Rev. B **32**, 3586 (1985).
- ¹⁹B. N. J. Persson, Phys. Rev. B **44**, 3277 (1991).
- ²⁰B. N. J. Persson, Surf. Sci. **269/270**, 103 (1992).
- ²¹S. Aubry and C. Andry, in *Proceedings of the Israel Physical Society*, edited by C. G. Kuper (Hilger, Bristol, 1979), Vol. 3, p. 133.
- ²²J. B. Sokoloff, Phys. Rev. B **42**, 760 (1990).
- ²³J. B. Sokoloff, J. Appl. Phys. **72**, 1262 (1992).
- ²⁴J. A. Barker, D. Henderson, and F. F. Abraham, Physica **106A**, 226 (1981).
- ²⁵W. E. Campbell, Trans. ASME **61**, 633 (1939).
- ²⁶J. M. Carlson and J. S. Langer, Phys. Rev. Lett. **62**, 2632 (1989).
- ²⁷H. Lamb, *Hydrodynamics* (Cambridge University, Cambridge, 1932).
- ²⁸Olof Eklöf, *Fysikhandboken* (Biblioteksförlaget, Stockholm, 1968).
- ²⁹D. Tabor, J. Appl. Phys. **16**, 325 (1945).
- ³⁰J. Boyd and B. P. Robertson, Trans. ASME **67**, 51 (1945).
- ³¹A. Sonntag, Electro-Technol. (N.Y.) **66**, 108 (1960).
- ³²J. Krim, D. H. Solina, and R. Chiarello, Phys. Rev. Lett. **66**, 181 (1991).